DUAL-BAND LIGHTWEIGHT, LOW-COST RF FRONT-END SOLUTIONS FOR POINT-TO-POINT WIRELESS APPLICATIONS

A Dissertation
Presented to
The Academic Faculty

By

Aida L. Vera López

In Partial Fulfillment
Of the Requirements for the Degree
Doctor of Philosophy in the
School of Electrical and Computer Engineering

Georgia Institute of Technology
August, 2015

DUAL-BAND LIGHTWEIGHT, LOW-COST RF FRONT-END SOLUTIONS FOR POINT-TO-POINT WIRELESS APPLICATIONS

Approved by:

Dr. John Papapolymerou, Advisor
School of Electrical and Computer Engineering
Georgia Institute of Technology

Dr. Z. John Zhang
School of Chemistry and Biochemistry
Georgia Institute of Technology

Dr. John D. Cressler
School of Electrical and Computer Engineering
Georgia Institute of Technology

Dr. Hua Wang
School of Electrical and Computer Engineering
Georgia Institute of Technology

Dr. Andrew F. Peterson
School of Electrical and Computer Engineering
Georgia Institute of Technology

Date Approved: May 28, 2015

To those who create and inspire creation

ACKNOWLEDGEMENTS

Through the years working towards my degree, several people provided vital resources and support that enabled me to finish, and keep my sanity in the process. I would like to extend my gratitude for their influence and impact. Firstly, I would like to acknowledge my professors in Mayagüez who challenged me to pursue my curiosity beyond my bachelor's degree. My research advisor, Dr. Papapolymerou, thanks for your continued support, patience and guidance. All my research project sponsors, as they certainly offered interesting problems and the necessary funding to find solutions for them. To the GEM Fellowship and Goizueta Foundation for their financial support. To all my Mirctech labmates, past and present, for their training, their questions, their conversations, shared laughs and coffee chats. To my family in Puerto Rico, for from a distance conveying the precise words to keep me going. To my extended family in Atlanta who effortlessly and consistently helped make Atlanta more than just a city, now a second home. To all the adversities I was fortunate enough to endure. I never anticipated their arrival, but now welcome their teachings and changes. Finally, to that invisible yet undeniable driving force that enabled the culmination of all my work. To you all, my appreciation, love and everlasting respect. Thank you.

TABLE OF CONTENTS

LIST OF TABLES

LIST OF FIGURES

SUMMARY

The objective of this work is to achieve the integration of a state-of-the-art RF CMOS chip in lightweight multilayer-organic (MLO) substrates at millimeter-wave frequencies. To do this, first the substrates need to be characterized above 30 GHz. This was done through the Ring Resonator Method. Once the loss and dielectric properties were known, the layers for the MLO stack-up were chosen and two different antenna arrays were designed for the chip's communication. Subsequently, a hybrid integration with a silicon interposer layer was developed in preparation for the future CMOS chip. This integration consisted of a combination of flip-chip bonding assisted by a non-conductive film (NCF) layer to secure the bonding. Finally, since the chip has two different operating frequencies, an exhaustive orientation study for the arrays was performed. The study revealed the best orientation for the antennas in order to minimize interaction between them in the package. The final package possesses the ability to simultaneously excite both array designs, and also includes all interconnects and transitions required by the RF CMOS chip. Although the main focus is at millimeter-wave frequencies, other novel techniques at different frequencies are discussed, such as utilizing microfluidic channels to reduce the size of RF designs, characterizing 3D-printing materials, and designing the first micro-dispensed antenna in Ka band. All of these help to highlight the ability and versatility of organic substrates at high frequencies.

CHAPTER 1:
BACKGROUND AND LITERATURE SURVEY

1.1 Introduction

Maxwell's unified equations are the foundation of electromagnetic theory. Through them, the concept of current radiating and producing electromagnetic waves has been used to enable modern communications. In particular, wireless telecommunications are the most commonly used technology today. There is, of course, a high demand for both novelty and improvement of the devices that support these communications. President Obama released the Wireless Innovation and Infrastructure Initiative in 2011, with the incentives of doubling the available wireless spectrum and drive wireless technology innovation [1]. To accomplish the task of providing broadband communications to the masses, several things are needed. As lower frequency bands become congested, and higher data rates are required, the need to move up in frequency becomes imperative. This move will certainly provide a more efficient use of the frequency spectrum and allow for better performance of point-to-point communications. In order to smoothly transition to higher frequencies, research needs to focus on the proper design and planning of millimeter-wave frequency structures, which inherently provide packaged solutions with superior performance. Work is also needed in characterizing the materials at these frequencies, integration and orientation planning, and studies of the transitions and packaging solutions for all devices involved.

The objective of this work is to achieve the integration of a state-of-the-art RF CMOS chip in lightweight multilayer-organic (MLO) substrates that yield superior performance to regular CMOS substrates and on-chip solutions. Using organic substrates will enable complete integration of broadband antennas at different millimeter-wave frequencies (57 and 80 GHz) in the system package. The package will also possess the ability of simultaneously excite both designs. The complete package includes directive dipole arrays and all interconnects and transitions for the RF CMOS chip. Attention was placed on the characterization of substrates used in the MLO package, the antenna designs and transitions, and optimizing the overall performance of the completed structure. Although the focus for the package integration is at millimeter-wave, the integration may be done at lower frequencies and some studies of techniques have been conducted.

1.2 Background of the Problem

As common frequency communication bands grow in useage and become more saturated, exploring higher frequencies for future communication devices becomes important. The unlicensed 60 GHz millimeter-wave band has become increasingly popular in serving this purpose. Moving up to higher frequencies, W-band (75 to 110 GHz) also compromises high data rate throughput. Antennas, filters and other RF components' performance varies considerably as frequency increases. This variation may be studied through the properties of the specific substrate material the component is made of. Relevant RF material properties, such as dielectric constant and loss tangent, are frequency dependent [2-4]. Therefore, to improve device modeling at higher frequencies, and thus, the performance of the final fabricated device, it is essential to study the properties of the material at those specific frequencies. Over the last few years, point-to-point communications with fast transfer speeds for demanding downloads to mobile devices have become an essential application. These require antennas with greater bandwidths to ensure high data rates. Better bandwidth performance has sparked great interest in Wireless Personal Area Networks (WPANs). Also, the inherently smaller size of devices at these frequencies, make them ideal for integrating into an existing package or chip. However, in doing so, the main difficulty lies in keeping good performance once the device is completely packaged. It is challenging to avoid the many losses intrinsic to millimeter-waves and keep production costs low. Two main packaging solutions have been studied

to integrate designs with the rest of the package. Both of the solutions will be discussed below.

PACKAGE INTEGRATION: ON-CHIP VS IN-PACKAGE

Antenna-on-chip (AoC) technologies have gained popularity as a way to package antennas with various RF front-end circuits on the same chip. While such devices possess the entire structure in one chip, many things have to be considered to maintain good radiation performance. The high dielectric constant of die substrates reduces antenna efficiency and thus, some processing is required to lessen this effect. Micromachining an air cavity, thinning down the substrate, and superstrate focusing, are a few commonly used techniques to improve radiation [5]. However effective, these techniques require additional fabrication steps and processing time, which usually translates into a more costly structure. Moreover, the actual size of the die also limits the achieved performance, making the overall design more difficult. A more suitable solution that has been studied to provide the adequate environment for these designs is Antenna-in-Package (AiP). An in-package solution has the versatility of integrating several substrate layers to yield the desired RF performance and incorporate any chips in the multilayer stack-up. Antenna-in-Package has been integrated through wirebonds at 60 GHz [6]. These bonds, while providing a considerable amount of loss at millimeter-wave frequencies, are relatively straightforward and well understood. To minimize the parasitics that arise from this method, flip-chip bonding may be

used. This bonding technique provides greater bandwidth and has been shown to yield good results at 60 GHz [7].

Previous studies have mainly focused on the integration of a single antenna frequency band and analyze how to individually incorporate packaged antenna designs, through interconnects into a chip [8]. Some work has also been done on how to switch several rotated copies of the radiating element to attain the desired orientation for the radiation patterns [9,10]. It is, however, more efficient to fully exploit the capabilities of the substrate materials and package more than one antenna design on the organics and incorporate the transceiver chip into the organic package. This will allow simultaneous communication for different frequency designs. Ultimately, there will be an increase in the data rate and this will help achieve an interactive transfer. Careful planning must be done to ensure performance is not compromised while including designs operating at different frequencies on a single package. New advances in package integration headed in this direction are discussed in the next section.

1.3 Recent Developments in Integration

With worldwide access to all kinds of mobile structures, the increasing demand for faster download speeds and smaller, more efficient devices grows. Not surprisingly, great attention is placed on millimeter-wave frequencies to provide short-range communications capable of multi-Gbps transfers. Several advances in RF-front ends using organics focus on wire-bonding the SiGe or GaAs chip onto the package. Examples of these techniques have been reported around the 60 GHz unlicensed band [11,12]. In [11], this is implemented in a System-on-chip (SoC). As previously noted, this may require more steps to achieve the desired radiation properties. These studies focus on transmit or receive packaged RF-front end module. Research on a full integration, including the RF CMOS chip packed on organics with all transitions and routing lines, is scarce, especially at millimeter-wave frequencies. Yet, numerous applications can benefit from this, particularly those with simultaneous two-way data transmission, including internet access and movie downloads (high definition video streaming). Appropriate for full-duplex communications, dual-frequency retrodirective arrays at different frequencies have been studied below 10 GHz [13,14]. Having the transmitting and receiving arrays at different frequencies (RF decoupled), possess the added benefit of substantially increasing the efficiency of the system which may require a high-frequency retrodirected signal by implementing a lower frequency interrogator signal [14]. However, proper planning of the integration and system design are needed to guarantee good radiation, as pattern shape may become distorted and gain value may drop.

Furthermore, having designs for such applications fully packaged can also provide an integrated solution for chip-to-chip communications.

Transceivers with multi-modality capabilities at 57 and 80 GHz have been successfully integrated [15-17]. These have focused on an on-chip solution with two separate outputs. An example is presented in Figure 1. Silicon and other electronic substrates have been used to integrate radio circuits at millimeter-wave frequencies with good results [18-20]. Ceramics have been widely used for antenna integration and packaging at these frequencies [21]. Low-temperature co-fired ceramic (LTCC) multilayer technology has both the maturity and stability to yield good performing devices. It has been successfully used to package antennas for transceivers at millimeter-wave frequencies [22,23]. Nonetheless, if integrating a full system, LTCC's lamination temperature of 800 ^{0}C would damage the IC's in an embedded scheme. Alternatively, organic substrates provide better RF properties without the need to further process them. Liquid crystal polymer (LCP) is an organic substrate that possesses low dielectric constant and loss, up to 170 GHz [2,24]. It is both conformal and near-hermetic. Compared to other CMOS substrates, LCP also has the great advantage of a significantly lower lamination temperature (285 ^{0}C) that will not damage the components. Making use of multilayer organic (MLO) substrates at these frequencies allows for optimal integration, while also reduces production costs. Si-based integrated circuits have been successfully embedded in low-temperature multi-layer organic substrates at W-band with record low interconnect loss [25]. LCP and RO3003™ are attractive substrates precisely because of these

capabilities. Ideally, the end result should be a good performing device that is easily integrated with other RF and electronic components. In this aspect, organically packaged RF-front ends have been successfully demonstrated at millimeter-wave frequencies [12,26].

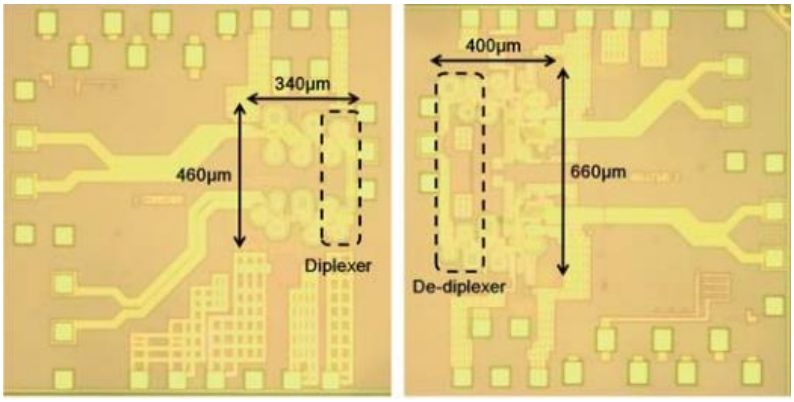

Figure 1. Integration application for CMOS chip-to-chip communication [17].

There is one aspect that cannot be overlooked when packaging radiating structures. It pertains to the orientation and relative distance between the radiating elements. This is particularly relevant when different operating frequency devices are involved (case depicted in Figure 1). Antenna orientation and placement affects the radiation patterns. Several, more involved techniques or components may be incorporated into a design to alleviate this interaction. Switches or circulators can be used, though these provide a specific amount of isolation and may also increase system loss and size. Increasing the distance between the radiating elements also helps. If one seeks to have a small package, increased distances may not be the best solution. Alternatively, a study of the antenna

orientations and how these affect the interaction with nearby reflectors may be done. This is particularly similar to what would be seen with a full-duplex communication system. Figure 2 shows our concept for the complete package to enable chip-to-chip communications at two different millimeter-wave frequencies.

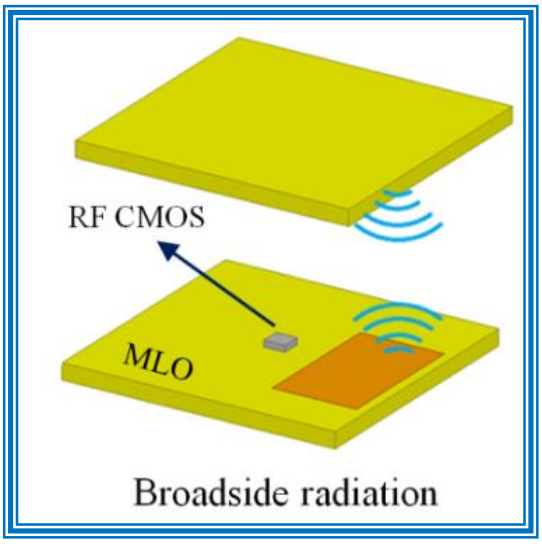

Figure 2. Concept for completely packaged RF CMOS on MLO substrates for dual frequency applications [27] with broadside antenna designs.

CHAPTER 2:
RF MATERIAL CHARACTERIZATION

Several studies were completed to evaluate the performance of organic substrates for millimeter-wave point-to-point communications and 3D-printed substrates in Ka-band (26.5 to 40 GHz). This research has focused in three major areas: high-frequency characterization of organic substrates, development of low-cost and lightweight antennas for millimeter-wave applications, and techniques to improve performance (packaging integration and orientation studies). The first portion relates to dielectric characterization and the following study was presented at the 60th Electronic Components and Technology Conference [28].

2.1 Thin Substrate Dielectric Characterization at Millimeter-Wave

The focus of this study is divided into two parts: material characterization and RF performance assessment. For the first part, the Ring Resonator Method was used. Through the analysis of its response in frequency, this method has the advantage of providing results over a wide frequency range and has proven to be accurate and effective in measuring substrate permittivity [29]. The technique was used to characterize three materials: RO3003™, RXP1HF and RXP4; from 30 GHz to 67 GHz. RO3003™ has been previously characterized up to 18 GHz with the Ring Resonator Method [29]. Both RXP1HF and RXP4 are new substrates developed by Rogers Corporation and their RF performance at higher frequencies has not been studied by the ring resonator method. These have been characterized up to 110 GHz through cavity resonators [30]. Contrary to [30], the RXP1

in the present study is a halogen free (HF) thin core substrate designated as RXP1HF. The RXP materials combination hold great relevance in that they possess low losses, are thin, PCB compatible, multilayered, and complementary to LCP. The latter (LCP) has gained popularity for its low cost, good performance, and conformal nature [2-4]. Table 1 presents available data for these materials from the manufacturers.

Table 1. Reported material properties

Material	f (GHz)	ε_r	tan δ	Source
RXP1HF	10	3.85	0.0050	Rogers
RXP4	10	2.90	0.0030	Rogers
RO3003	1	3.00	0.0013	Rogers

To create the ring resonator designs, several constraints were considered. Among these, the impedance of the resonator, which should be chosen such that the ratio $w/r < 0.2$; where w is the width of the resonator, and r is mean radius of the ring resonator [31]. This is done to avoid the excitation of higher order modes. The two resonator impedances selected were 60, and 70 ohms. Two frequencies spectrums were chosen for each material, one spaced every 8 GHz, and the other every 10 GHz. The designs based on the selected impedances and resonant frequencies are illustrated in Table 2. Once these were known, the mean radius of each resonator structure is determined by using Equation (1)

$$f_0 = \frac{nc}{2\pi\ r_m \sqrt{\varepsilon_{eff}}} \qquad \textbf{(1)}$$

where f_0 is the nth resonant frequency, r_m is the mean radius, ε_{eff} corresponds to effective dielectric constant of the material, and c is the speed of light in vacuum. The diameter of the ring-resonator must also be larger than the λ of the lowest frequency in the bandwidth of interest [29].

Table 2. Resonator designs

Design	Mean Radius (mm)	Resonator Impedance (Ω)	Resonance (GHz)
A	3	60	10
B	4		8
C	3	70	10
D	4		8

Coplanar-to-microstrip transitions were designed for the 30-67 GHz bandwitdth [32]. To keep coupling at a minimum, the spacing between the microstip line and resonator was optimized using Ansoft's High Frequency Structure Simulator (HFSS) to achieve a transmission coefficient S_{21} below -20 dB throughout the bandwidth. Figure 3 shows the resonator structure with transitions.

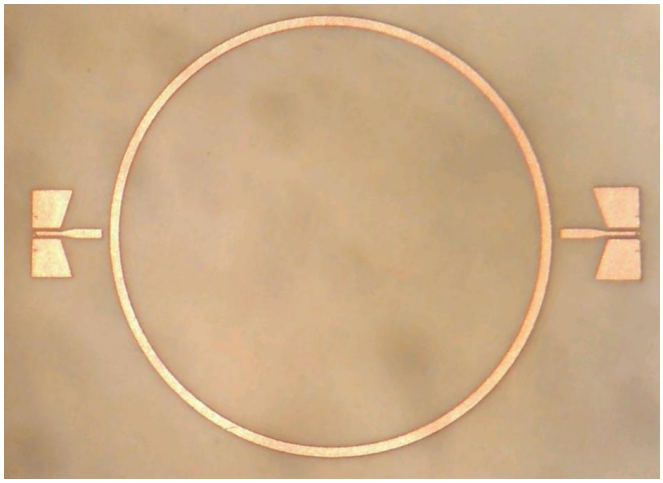

Figure 3. Ring resonator with coplanar-to-microstrip transition.

RESONATOR MEASUREMENTS

TRL-calibration is required prior to the measurements of all ring resonators [33]. For this, a set of four lines was designed, a thru and a reflect standard. Each of the lines, according to their length, covers a portion of the 30 to 67 GHz bandwidth under study. This relation is governed by the following equations:

$$l_i = \frac{v}{12 f_{Li}} \qquad \textbf{(2a)}$$

and

$$v = c \Big/ \sqrt{\varepsilon_{eff}} \qquad \textbf{(2b)}$$

where i=1,2,3…n; v is the propagation speed, ε_{eff} is the relative effective dielectric constant, c is the speed of light in vacuum, and f_{Li} is the lowest frequency of band i. When

measurements were taken, the parasitic effects found through the transitions were factored out in calibration.

RING RESONATOR CHARACTERIZATION RESULTS

Frequency dispersion effects were not accounted for to calculate the relative permittivity of the materials. Surface roughness for electrodeposited metallization was measured to be 1.89 μm. The error bars presented for each data point were calculated based on the guidelines described in [34]. The measured relative permittivity and loss tangents for all materials are presented in Figures 4 thru 6. Figure 4 shows results for RXP1. The dielectric constant increases from 3.85 to 4.20 and the loss tangent increases from 0.005 to 0.0065, which agrees with [30]. RXP4 exhibits a slight change in dielectric constant (Figure 5(a)), with value ranging from 3.09 to 3.15. The loss does not exceed 0.005 (Figure 5(b)). RO3003™ displays a small increase in dielectric constant with frequency (Figure 6). Its loss stays below 0.003, making suitable for mm-wave applications. A summary of all measured results is found in Table 3.

Table 3. Summary of ring resonator results

Material	ε_r	tan δ
RXP1	4.21 ± 0.065	0.0065 ± 0.0160
RXP4	3.13 ± 0.040	0.0040 ± 0.0100
RO3003™	3.08 ± 0.050	0.0021 ± 0.0083

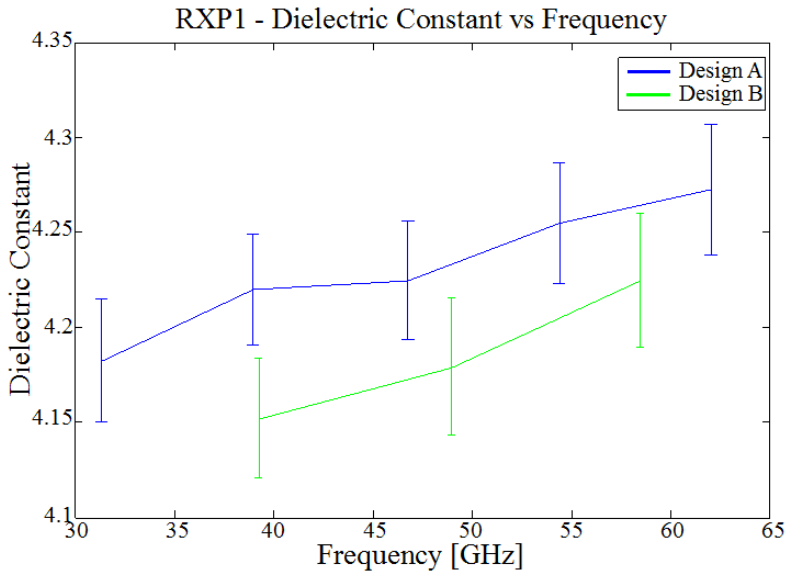

(a)

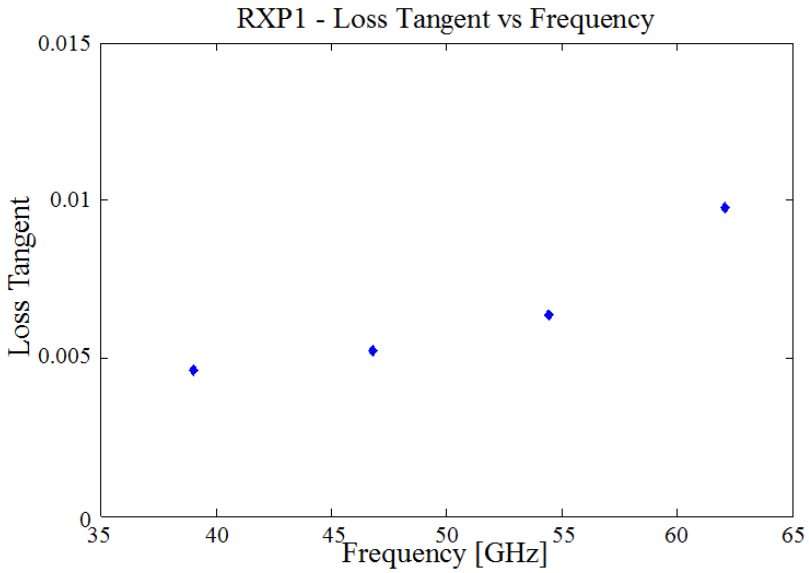

(b)

Figure 4. RXP1 results: (a) dielectric constant and (b) loss tangent, from 30 to 67 GHz.

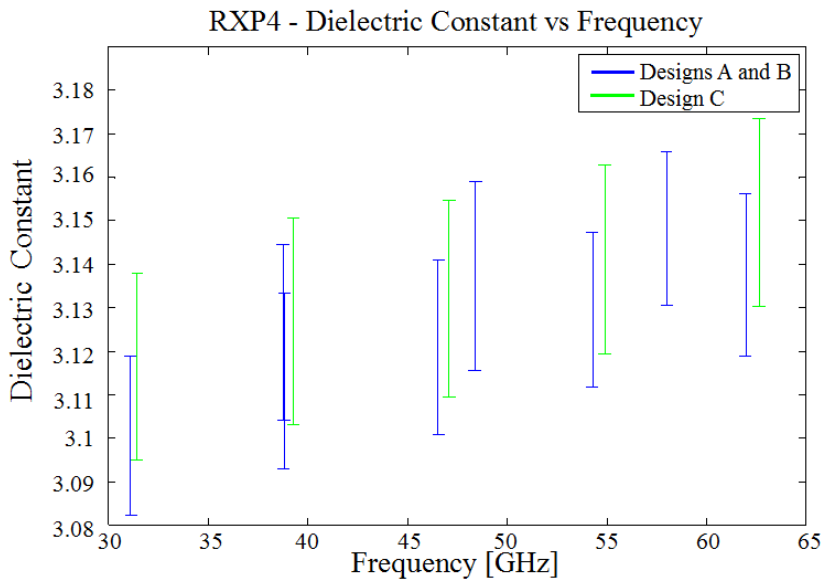

(a)

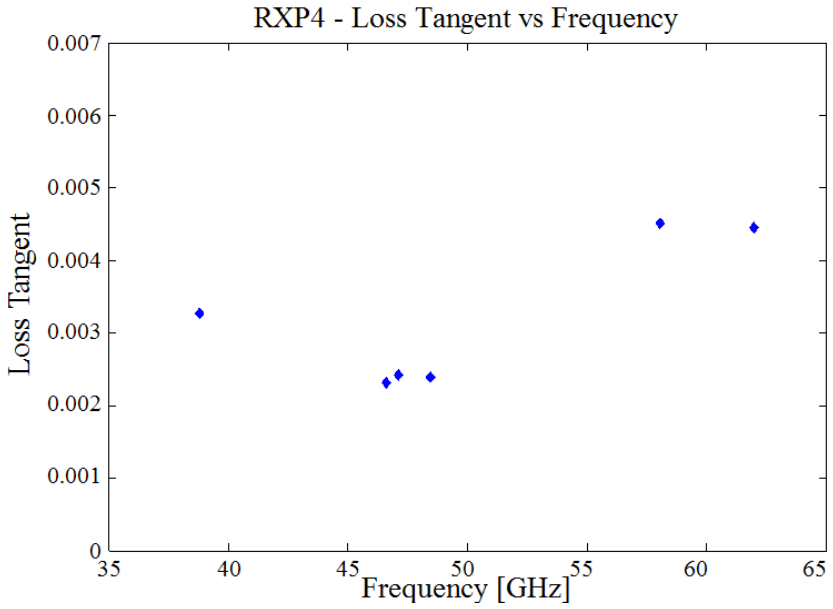

(b)

Figure 5. RXP4 results: (a) dielectric constant and (b) loss tangent, from 30 to 67 GHz.

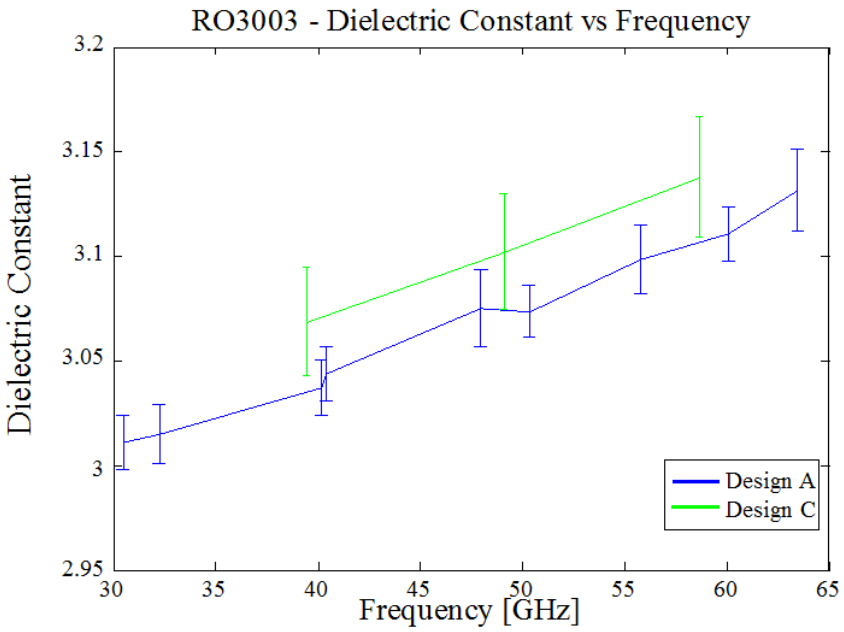

Figure 6. RO3003 dielectric constant from 30 to 67 GHz.

2.2 3D-Printing Polymer-based Substrate

3D-printing fabrication methods have received a great deal of attention in recent years. This is not surprising as these techniques possess the ability to create a broad range of devices in a time saving, relatively inexpensive fashion. Great versatility arises not only from the actual devices created, but also from the ability to integrate them with other electronic structures [35]. RF devices would greatly benefit from the capabilities this fabrication method provides, especially when compared to other more involved techniques. However, there is limited information on the RF performance of those commonly employed materials used with this method (mainly plastic materials), particularly at higher frequencies. Such information is vital for material selection and design performance. Acrynolitrile Butadiene Styrene (ABS) is a thermoplastic that is very suitable for the fused deposition modeling process [36], and is also commonly used in injection molding to produce a variety of industrial and consumer products. This material has good overall mechanical properties and is printed at relatively low temperature (270 °C), when compared with other printable polymers. Also, it presents no hazards to human health.

A detailed study of several plastic materials' RF properties over temperature provided data for ABS exactly at 11 GHz. This study used a cylindrical cavity resonator to characterize the materials [37], although it does not to mention the origin of the material or the thickness of the analyzed sample. Another characterization investigation makes use of three different methods to provide data from 1 MHz to 11 GHz [38]. The ABS materials used are quite thick (7.63 mm), which makes them impractical for millimeter-wave applications. In [49], a Fabry-Perot cavity provides data at 60 GHz. However, the purpose

of ABS in the paper is for an antenna lens, not an RF substrate with metal deposited on it. A summary of reported ABS properties is found in Table 4.

Table 4. Reported RF properties for ABS

Material	**Reference**	**Dielectric Properties**		
		Frequency	ε_r	tan δ
Not specified	[36]	11 GHz	2.79	0.00905
M30 Lay	[37]		2.60	0.00980
M30 St	[37]		2.55	0.01300
Pure	[37]		2.54	0.01060
ABS-M30	[38]	60 GHz	2.48	0.00800

Despite the prior work, there are no reported studies that look at higher frequencies and thinner layers of ABS as an RF substrate to be printed on. Previous works have shown that this material can be used to realize antennas, obtaining good results [40]. As these 3-D techniques are able to move up in frequency with a resolution down to 200 μm [41], it is useful to investigate the material's behavior at these frequencies and the feasibility for circuit and antenna design. To investigate if ABS is a suitable material for millimeter-wave frequencies, a cavity resonator was employed to characterize the material above 10 GHz. Data acquired will later be used to design a patch antenna around 25 GHz, which is directly printed on ABS using thick-film Ag paste. Neither the thin layer characterization of ABS nor its use for antenna design has been done before above 11 GHz. Complete results of this study will be presented at the 2015 International Microwave Symposium [42].

CAVITY RESONATOR CHARACTERIZATION

To successfully carry out an RF design, it is important to first characterize the material at the desired frequency range. For this purpose, test samples were prepared using a Stratasys uPrint SE FDM printer, by printing multiple 250 µm layers until achieving the desired thickness. The substrate thickness relative to the operating wavelength must be carefully selected given its influence on resulting high frequency performance. If the thickness is too small the efficiency, gain and bandwidth of the antenna will suffer, and if too large, surface waves will diminish performance and cause spurious radiation. Keeping this and the Ka-band target frequency in mind, the chosen thicknesses for the study were ~550 µm and 850 µm. Finally, a cavity resonator was used to analyze the samples. Figure 7 depicts the setup used for these measurements.

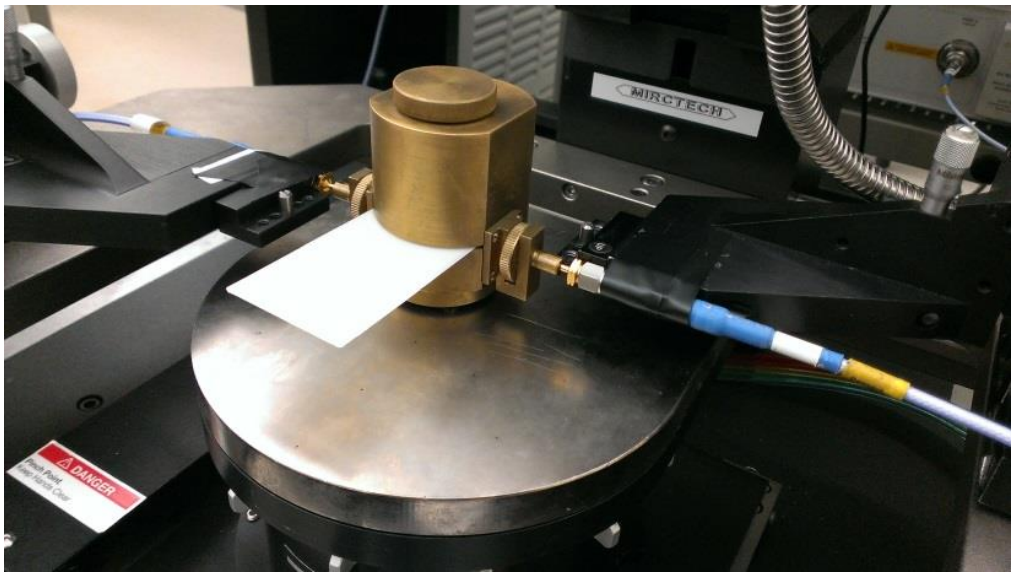

Figure 7. Measurement setup for cavity resonator with sample inside.

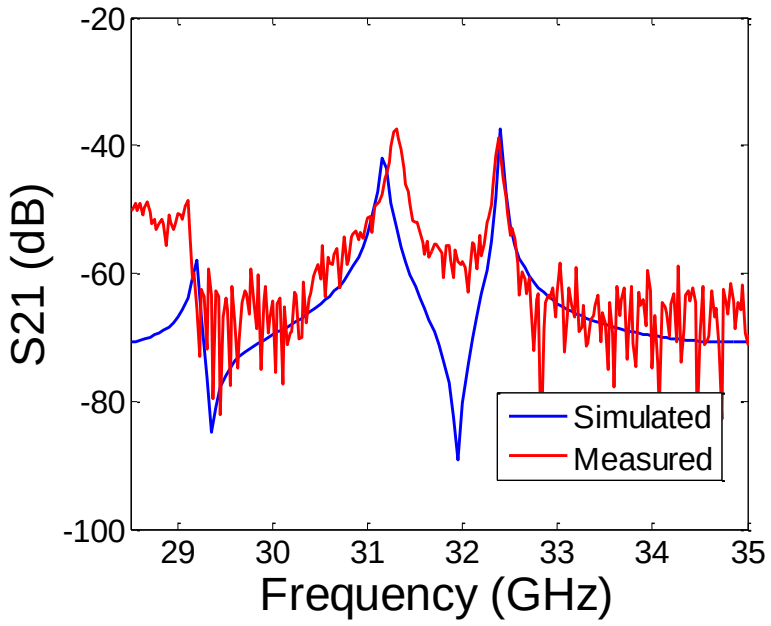

Figure 8. Cavity resonator results (S_{21} vs Frequency) for simulated and measured results.

A NIST SplitC Software was used to first estimate the resonance of the samples, based on the available data (at a lower frequency). The samples were measured, and note of available resonances was taken. Relevant information lies in the resonant frequency value (relates to dielectric constant) and its corresponding Q-factor (relates to loss). The measured values were analyzed with SplitC software, now to provide dielectric properties. A High Frequency Structural Simulator (HFSS) simulation of the cavity was then performed to verify these characterization properties. These results were compared with the measured ones. This iterative analysis provides the data for the material. Figure 8 shows good agreement between the measured and simulated results. Table 5 summarizes the

characterized values for the ABS samples around 30 GHz. Our results agree with those found in [36].

Table 5. Characterized properties for ABS

Sample thickness [μm]	**Dielectric Properties**		
	Frequency	ε_r	tan δ
575	~ 30 GHz	2.352	0.00668
835		2.386	0.00651

2.3 Effects on Antenna Performance

As a second part of the characterization studies in the previous sections, the obtained results were validated through antenna designs. This allows comparison between measurements and simulations, while providing actual RF performance information at higher frequencies.

2.3.1 Aperture-Coupled Patch Antenna

For the materials characterized in Chapter 2.1, aperture-coupled patch antennas were designed at 60 GHz using RXP1 and RXP4 materials. The simulated designs were done using the available data for the RXP materials at 10 GHz (Table 1). The design consists of five layers: radiating element, its corresponding substrate, ground with given aperture, a feed line, and its substrate. Figure 9 illustrates how these are distributed. First the dimensions of the patch were calculated. The width of the patch controls the resonant resistance of the antenna [43] and its value is roughly λ/2 at 60 GHz. The length of patch determines the resonant frequency. Both starting values were determined by the regular rectangular patch equations:

$$W_{patch} = \frac{c}{2 f_0 \sqrt{\frac{\varepsilon_r + 1}{2}}} \quad \textbf{(3a)}$$

$$L_{patch} = \frac{c}{2 f_0 \sqrt{\varepsilon_{eff}}} - 2\Delta L \quad \textbf{(3b)}$$

$$\Delta L = 0.412h \frac{\left(\varepsilon_{eff} + 0.3\right)\left(w/h + 0.264\right)}{\left(\varepsilon_{eff} - 0.258\right)\left(w/h + 0.8\right)} \quad \textbf{(3c)}$$

where ε_r is the substrate's dielectric constant, c is the speed of light in vacuum, f_0 is the resonant frequency, ε_{eff} is the effective dielectric constant, w is the width of the patch, and h is the height of the substrate. The length of the aperture greatly influences the coupling level achieved. Its length should be enough to ensure a good impedance match. The width of the slot is usually taken much smaller than the aperture length. To yield the highest coupling, the aperture is located at the center of the patch. The feeding mechanism used in the designs consists of a simple 50 ohm microstrip line that extends past the aperture.

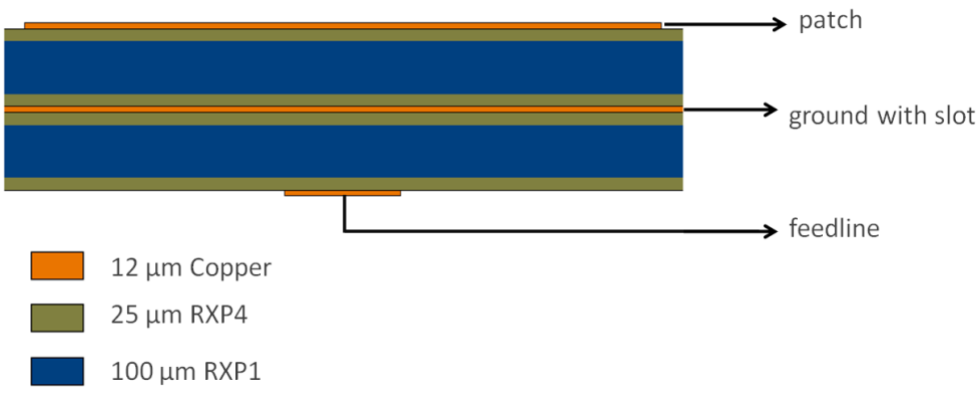

Figure 9. Aperture-coupled antenna cross-section.

ANTENNA DESIGN FABRICATION

RXP antenna was fabricated using standard lithography process. Individual layers were first laser ablated to form 1.5 mm diameter holes at four corners of each of the plies. These holes were threaded through a stainless steel mold to maintain layer to layer alignment. The lamination process is similar to the Low Temperature Co-fired Ceramics (LTCC). The laser drilled thin plies were patterned using a combination of positive and

negative resists. The copper features and the aperture were then carefully defined with controlled metal etch. Figure 10 depicts the defined aperture, and feedline. Lamination of the individual plies was done using an electrically heated lamination machine. The lamination conditions were 400 psi at 450C with gradual heating cycle under uniform pressure. The fabricated antenna was connected through a GPPO edge mount connector and measured with a network analyzer.

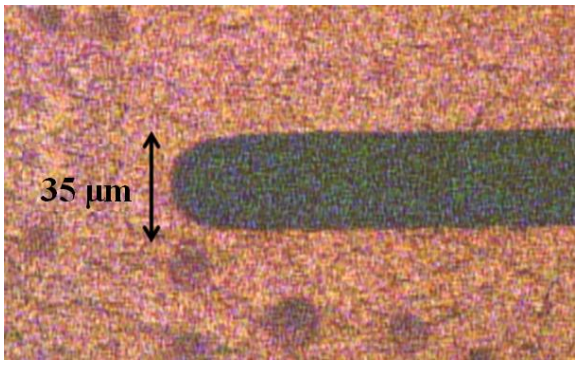

(a)

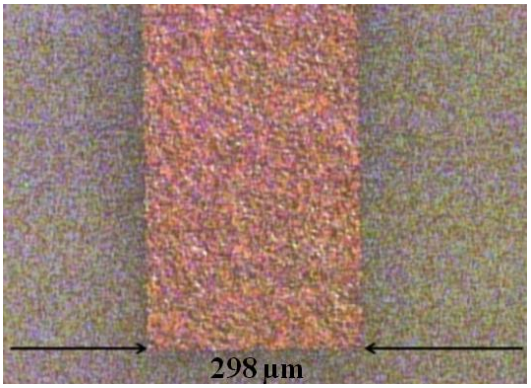

(b)

Figure 10. Fabrication results: (a) Ground aperture and (b) Feedline.

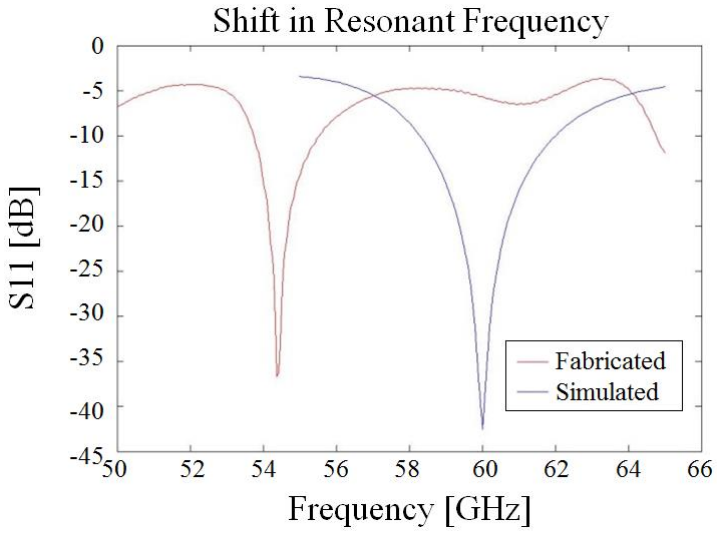

(a)

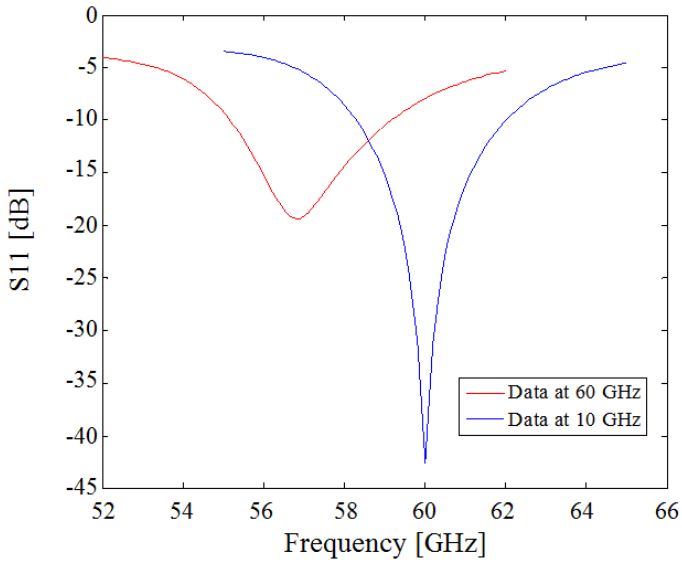

(b)

Figure 11. (a) Fabricated antennas' shift in frequency; (b) S_{11} results using 10 GHz and 60 GHz dielectric properties data.

Figure 11(a) shows a comparison between measured and simulated results. A frequency shift from 60 GHz to 54.4 GHz is observed. This displacement is attributed to using RXP data for lower frequencies, which have lower losses and dielectric constant. Measurements for both RXP1 and RXP4 showed an increase in dielectric constant with increasing frequency that is consistent with the frequency shift experienced in the antenna. A simulation with the measured dielectric data at 60 GHz was performed. The results of that simulation are shown in Figure 11(b), which shows a shift in frequency from 60 to 56.8 GHz. The remaining difference is due to variances in substrate thickness. This serves to demonstrate and emphasize the importance of characterization in RF design.

2.3.2 Micro-Dispensed Patch Antenna

A Ka-band antenna was designed using the results of the cavity resonator characterization for ABS material in Chapter 2.2. This one was directly printed on top using silver ink. Focus was placed on designing the antenna for a ~850 μm thick ABS substrate. As with any traditional patch antenna design, its resonance is controlled by the length (which depends on the frequency and dielectric constant). The width of the patch is roughly $\lambda_{eff}/2$. These values were calculated and a quarter-wave transformer was used for impedance matching. Values were then optimized using an HFSS model. This yielded dimensions close to 3.0 mm for the patch.

3D-PRINTING FABRICATION

The antenna was fabricated using a two-step process combining fused deposition modeling (FDM) and the direct print additive manufacturing (DPAM) micro-dispensing

method. The 835 micron-thick ABS substrate was produced using a Stratasys uPrint SE FDM printer and an ABS filament diameter of 1.75 mm. Using the minimum single layer thickness of approximately 250 microns, there are 3 layers that comprise the substrate. An nScrypt 3Dn-300 micro-dispensing tool was used to deposit the Dupont CB028 Ag thick-film paste for the top and bottom metallization. After conductor printing, the antenna was cured in an oven for 1 hour at 90° C. Finally, a Southwest Microwave model 1492-02A-5 connector was attached to the antenna feedline. The signal pin and ground connections were made using manually applied CB028 conductor, followed by a second cure cycle. Post-fabrication testing was performed to characterize the electrical and mechanical properties of the antenna. A profilometer scan of the top surface reveals a mean surface roughness of 86.2 μm (Ra), and an average conductor thickness of 42.2 μm. The measured conductivity of the Ag film is 1.65e6 S/m. The assembled antenna is shown in Figure 12.

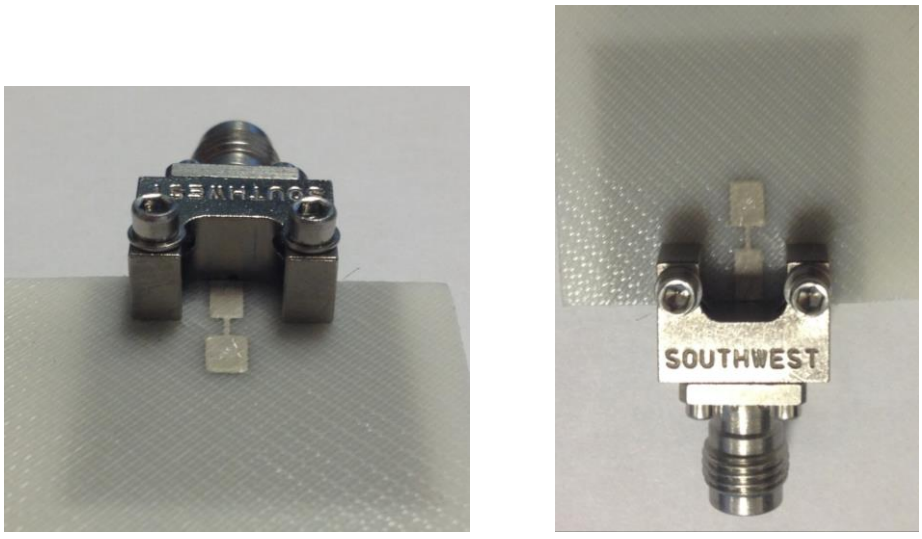

Figure 12. Fabricated patch antenna with connector.

MEASURED RESULTS

The fabricated antenna's S_{11} results are compared to simulated results in Figure 13. Both antennas resonate close to 25 GHz, and possess good agreement. The slight shift in frequency seen in the measured results is mainly due to the proximity of the connector and variations in fabricated dimensions. Normalized pattern cuts are found in Figure 14. Again, the effect of the connector is predominantly seen in E-the plane (as connector is in this plane).

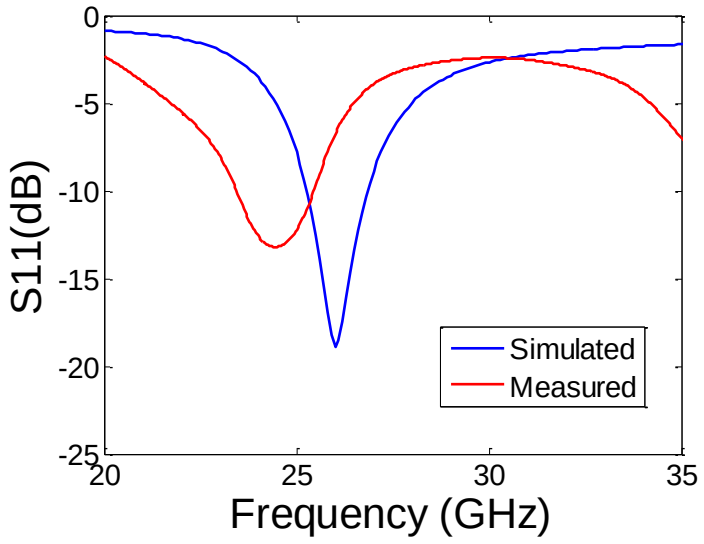

Figure 13. S_{11} vs Frequency comparison for measured and simulated designs.

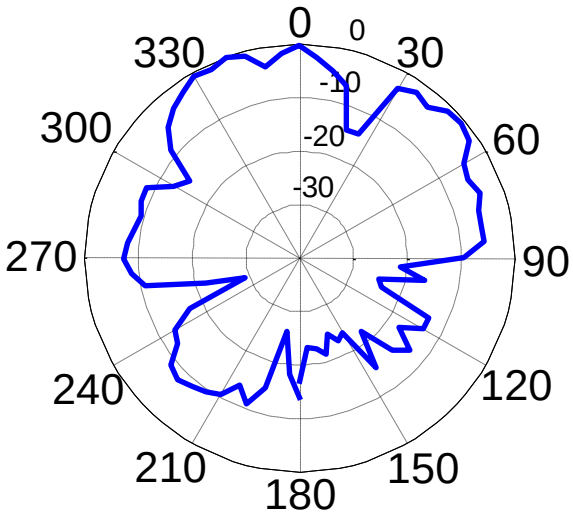

(a)

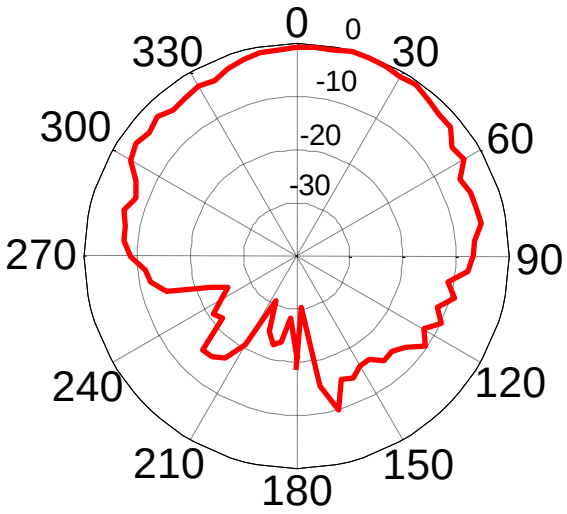

(b)

Figure 14. Normalized measured radiation pattern cuts: (a) E-Plane and (b) H-Plane.

With the characterized properties obtained above 11 GHz for ABS, a working antenna design was successfully achieved through micro-dispensed technology (the first design in that frequency range). Great novelty resides in directly depositing ink onto the ABS substrate at this frequency. These results speak not only about the potential of ABS as an RF substrate, but also open the possibilities of 3D-printing RF structures at mm-wave frequencies.

CHAPER 3:
NOVEL PACKAGING AND ANTENNA TECHNIQUES

Several different novel techniques were developed along the research course to find the best solution for the final integrated package. In this chapter, all of these are discussed in detail and results are provided as validation of their success. The first one consists of creating a microfluidic channel on organic substrates to insert high-dielectric fluids onto the stack-up, increase the effective dielectric constant and thus reduce the dimensions of the generated designs. This work was published in the 2013 Asia Pacific Microwave Conference [44].

3.1 Microfluidic Channel as Size Reducing Technique

As modern communications continually strive to produce smaller and more efficient devices, developing new antenna size reduction techniques becomes imperative. This is particularly relevant for lower frequency applications, as the wavelength is inherently larger. Size reduction can be achieved by modifying either the geometry of the radiating element or the environment in which it exists. By embedding the antenna's dielectric substrate with metamaterial structures, its magnetic permeability may be adjusted to yield a smaller antenna size [45]. Dielectric loading is another common method used, and can result in very broadband antennas. However, the loading slabs may cause the antenna to exhibit too high a profile for conformal, height-constrained applications [46]. Other common techniques include significant meandering of the radiating element [47], or the use of fractal geometries to efficiently utilize a given area [48]. Of course, it is well known that a high dielectric constant substrate can also be used to reduce the size of an

antenna. While this is often a good starting point for antenna miniaturization, in order to achieve significant reduction at megahertz frequencies, the designer may require a substrate with even higher dielectric constant than conventional RF substrates, such as that possessed by some fluids.

Below 2 GHz, the dielectric constant of water is about 80 [49], and the loss tangent is around 0.06 [50], making it an ideal candidate as a substrate for planar and compact low frequency antennas with good efficiency. To utilize water in this manner, a nearly hermetic base material is required in which to create a channel. Organic substrates such as liquid crystal polymer (LCP) and Rogers' RO3000™ series have proven multi-layer capabilities, with good performance up to mm-wave frequencies [51]. Also, with moisture absorption of less than 0.1% [52] they are ideal for near-hermetic sealing. Thus we present, for the first time, a microfluidic channel made in a multi-layer organic stack-up that enables the addition of high dielectric fluids for antenna miniaturization. It also provides significant versatility for integration with other multi-layered structures.

Table 6. Multi-layer stack-up description

Layer	Description	Material	Thickness
1	Radiating elements	Copper	18 µm
2	Membrane substrate	RO3003™	5 mil
3	Bond ply	ULTRALAM 3908®	1 mil
4	Support substrate	RO3003™	50 mil
5	Bond ply	ULTRALAM 3908®	1 mil
6	Sealing substrate	RO3003™	5 mil

To properly showcase the reduction attained, two different antennas were designed. The first one is a simple dipole highlighting length reduction and the second one is a loop antenna emphasizing overall area reduction.

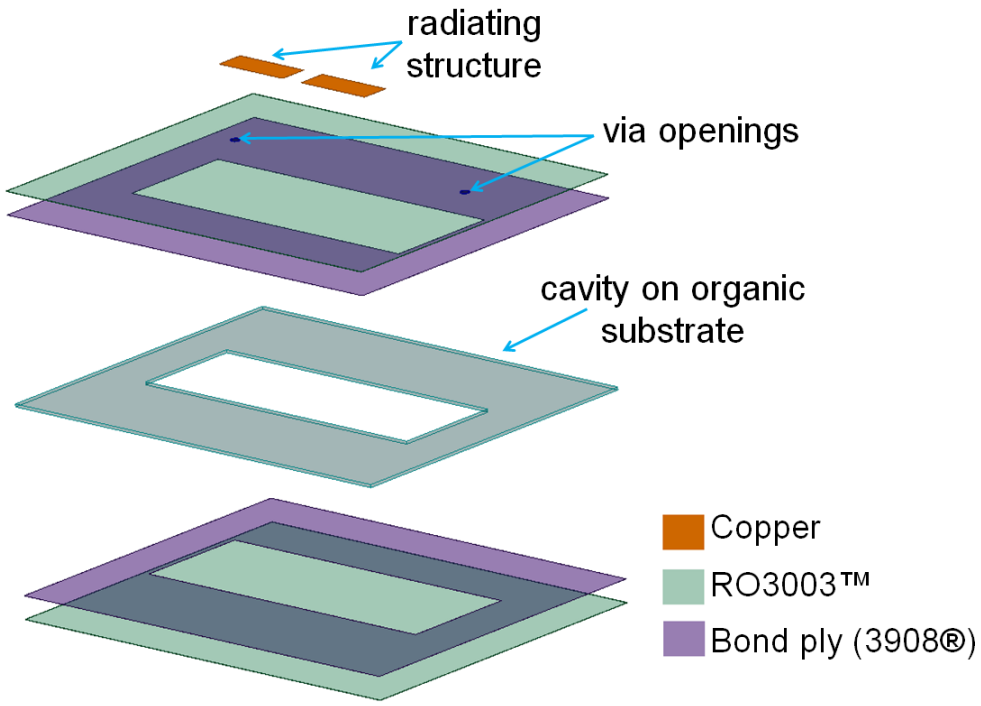

Figure 15. 3D-view of multi-layer organic stack-up with channel.

DIPOLE DESIGN

Two different half-wavelength dipoles were designed at 915 MHz: one on 50 mil Rogers' RO3003™ (ε_r = 3) substrate, and the other on a multi-layer organic stack-up with the microfluidic channel. This stack-up can be seen in Figure 15. Details on the layers used are found in Table 6. The overall length of the dipole on RO3003™ is 136 mm, while the one with the microfluidic channel has a length of 76 mm (with the channel practically full with distilled water).

LOOP DESIGN

To assess the extent of area reduction of the water-filled cavity, some simple rectangular loop antennas operating at 915 MHz were also designed. As in the dipole case, one loop antenna was fabricated on an unperturbed 50 mil RO3003™ substrate, while the other was fabricated on the same stack-up as shown in Figure 15. In full-wave simulations, it was found that for this type of antenna, and for a given substrate height and trace width, the aspect ratio (L/W) had the largest effect in impedance matching. For a trace width of about 5 mm, in order to improve matching, the channel antenna's aspect ratio was required to be near unity, while the non-channel loop's aspect ratio had to be closer to 2:1.

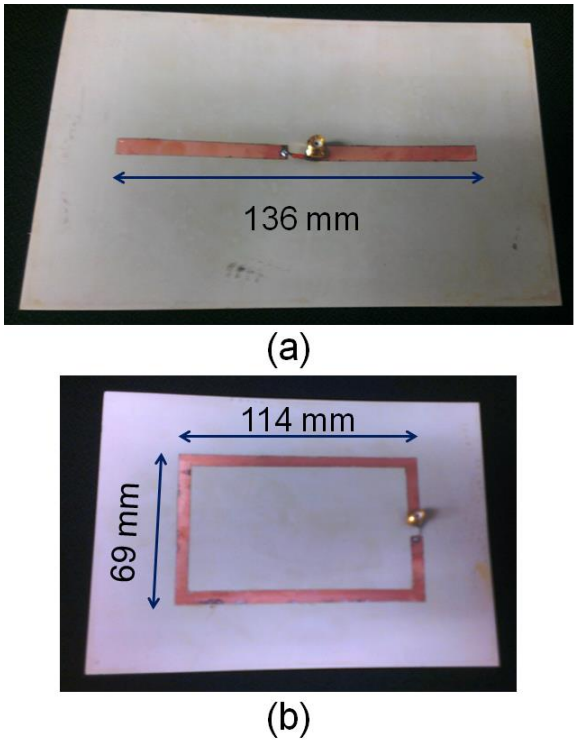

Figure 16. Top-view of fabricated designs without channel: (a) Dipole and (b) Loop.

A top-view of the planar dipole on the organic substrate is seen in Figure 16(a). In Figure 16(b), a top-view with dimensions of the loop design on the organic substrate without the channel is found.

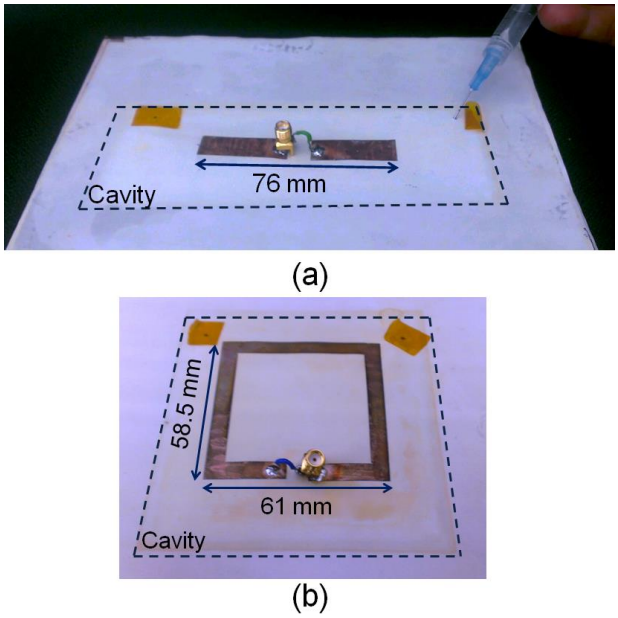

Figure 17. Fabricated designs with cavity: (a) Dipole and (b) Loop.

ANTENNA AND CHANNEL FABRICATION

The fabrication process of the designs without the microfluidic channel simply consisted of etching the features on top of the 50 mil RO3003™ substrate. The ones with the channel required additional drilling and bonding. First, a cavity on the supporting 50 mil RO3003™ substrate was drilled (layer 4 in Table 6). Then, the via openings were laser drilled on the top layer to allow access to the cavity. All the layers were then bonded using 1 mil Rogers 3908® as bond ply. The antenna features were then wet etched onto the top surface. Finally, a syringe was used to inject distilled water through the vias into the

microfluidic channels (Figure 38). An SMA connector is used for measurements, and as a balun (soldered to one end as ground). The length reduction for the dipole was approximately 44% (60 mm), while the area reduction for the loop was around 54% (4300 mm^2).

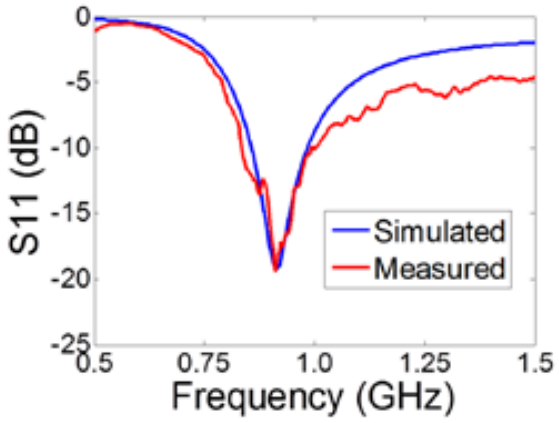

(a)

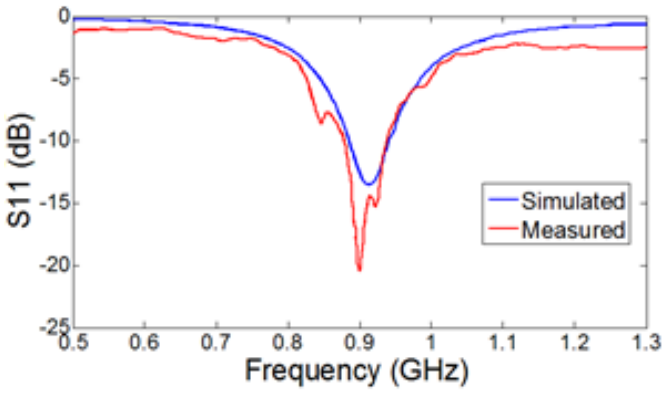

(b)

Figure 18. (a) S_{11} comparison for dipole without microfluidic channel; (b) S_{11} comparison for loop without microfluidic channel.

The fabricated antennas were measured using standard SMA connectors. The Agilent E8361C PNA was calibrated and used for the return loss measurements. First, the non-channel designs were measured. The results agreed extremely well with simulations, as seen in Figure 18(a) and 18(b). These results establish a baseline for comparison with the smaller, multi-layer designs.

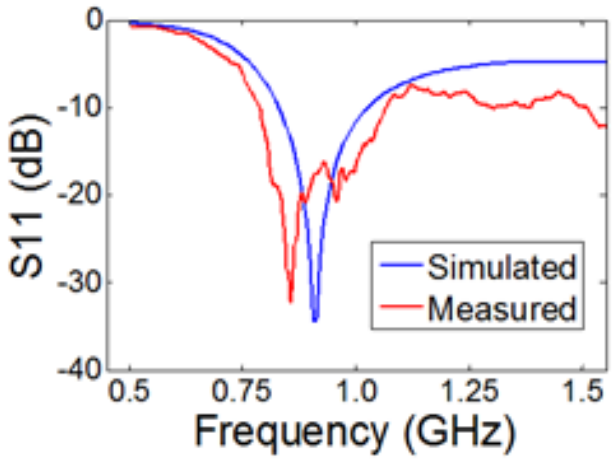

(a)

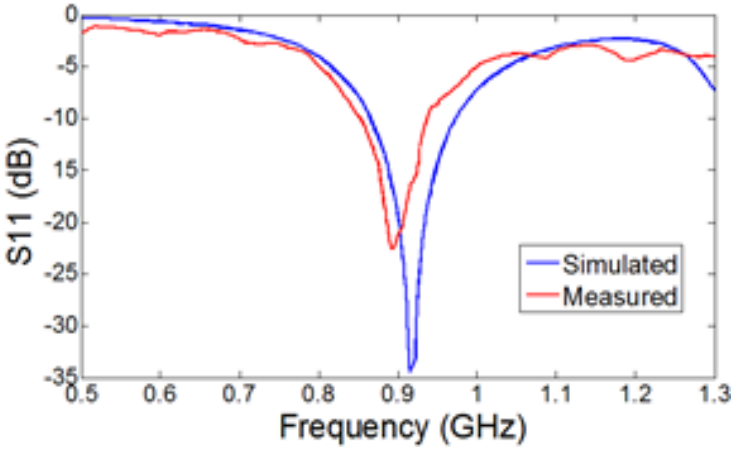

(b)

Figure 19. (a) S_{11} comparison for water-filled channel dipole design; (b) S_{11} comparison for water-filled channel loop design.

Figures 19(a) and 19(b) depict the S_{11} measurements for these designs. A slight shift in frequency due to an increase in the predicted water level can be seen, caused by the flexibility of the organic substrate. The dipole resonates at 865 MHz and the loop at 890 MHz. Both designs exhibit a broadband performance.

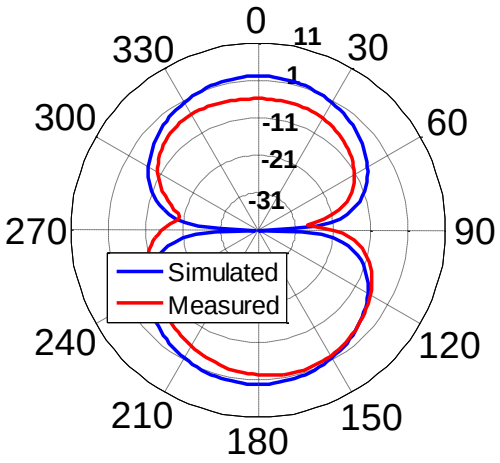

(a)

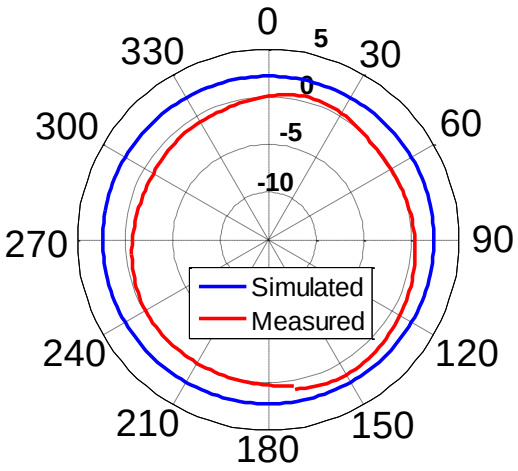

(b)

Figure 20. Microfluidic dipole radiation patterns: (a) E-plane and (b) H-Plane.

The measured E-plane and H-plane radiation pattern cuts for the microfluidic dipole are shown in Figure 20. These match the shape of the simulated ones very well. Differences in gain between measured and simulated patterns are mainly due to the connector used and measurement setup. Because of the omni-directional nature of the antenna, and its size compared to the connector and detector in the setup, some blockage occurs in the measurements and less gain is achieved as a result. There is a tradeoff between getting the correct shape of the pattern, and the right gain.

The created channel embedded in organic substrates helped significantly reduce the size of two radiating elements. The length reduction seen in the dipole is over 44% and the area reduction for the loop is 54%. Good performance was maintained on both designs, with over 10% bandwidth. Incorporating this simple and versatile technique with other proven reduction methods will further reduce the size and make designs at these frequencies quite compact.

3.2 On-Chip Antennas: Micromachined Patch Antenna

Efficiently integrating electronic circuits with RF devices is of outmost importance. Frequently used LTCC materials, such as gallium arsenide (GaAs) and silicon (Si), can be employed in RF designs. However, given their high dielectric constant, there is a need to suppress surface waves to achieve good performance, particularly for thicker substrate heights. Micromachined antennas have aided in this effort [53-55]. This part of the research, published in [56], focused on achieving a potential on chip antenna (on Si) at 60 GHz and studied the effect various thicknesses on antenna performance. To do this, an air cavity was micromachined. This one is centered directly underneath the radiating microstrip patch. The multi-layered structure consists of three dielectric layers. The first two layers (BCB and SiO_2) aid in the micromachining process. The antenna itself sits on top of a BCB and SiO_2 membrane (micromachined air cavity is below). Details of the layer properties are found in Table 7.

Table 7. Micromachined design layers and material properties

Material	**Layer Properties**	
	Dielectric constant	**Height (μm)**
BCB	4.0	11
SiO_2	2.6	0.2
Silicon	11.9	100 – 400

The dimensions of the patch were determined using equations 3a thru 3c. To ensure proper radiation, the dimensions of the air cavity were initially taken to be the size of the patch plus two times the height of the substrate [57]. At higher frequencies, it is best to avoid having large electric structures close to the radiating element. Therefore, a microstrip-to-coplanar transition was designed for probing [32]. Figure 21 illustrates the complete structure along with the transition.

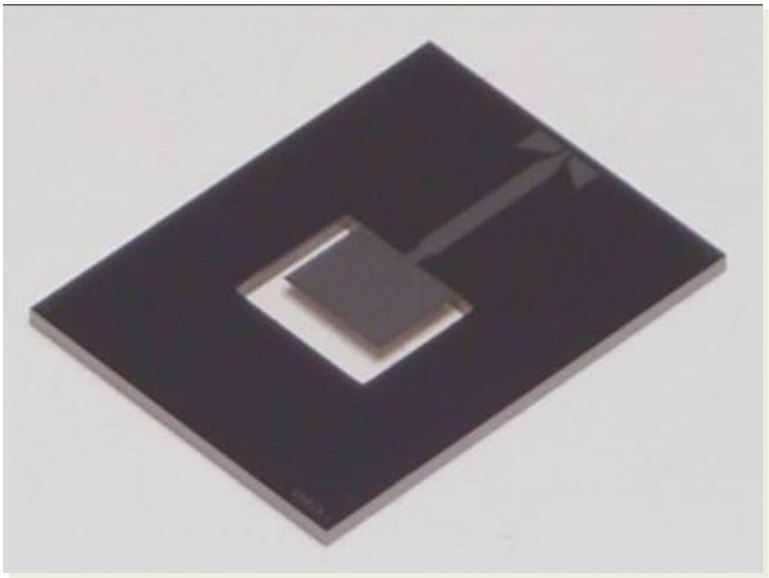

Figure 21. Fabricated micromachined patch antenna.

Several simulations were performed with different heights for the silicon substrate. Figure 22 illustrates these simulated results. The bandwidth (Figure 22(a)) naturally increases as we increase the substrate height, but the match becomes worse. This is clearly seen in the radiation patterns (Figure 22(b)), where we start to notice the surface wave effects in the 300 μm height plot.

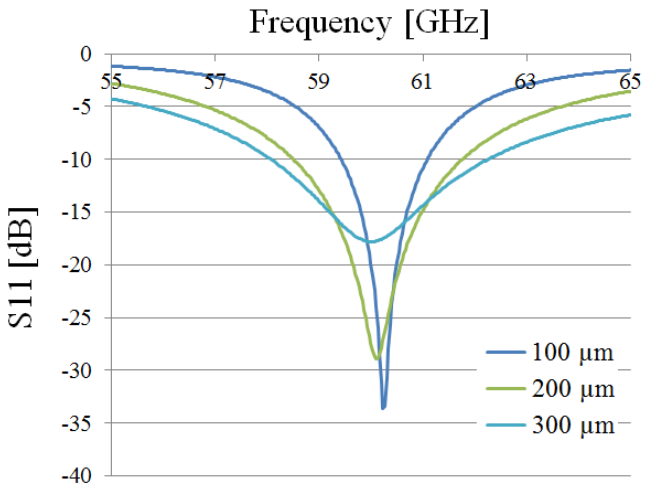

(a)

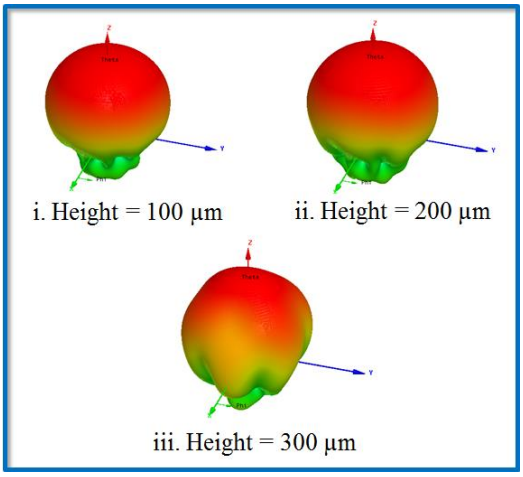

(b)

Figure 22. Simulated results for different heights: (a) S_{11} vs frequency; (b) 3D radiation patterns for Si heights 100 to 300 µm.

The available Si wafer height for this study was 400 µm. The fabricated structure and its measurements focused on this height. Figure 23(a) shows the measured S_{11} vs frequency. The simulated and measured results follow the same trend. There are a few more losses, likely due to slight fabrication differences and measurement sensitivity. Figure 23(b) shows significant distortion in the radiation pattern. This highlights the effect using a relatively thick substrate has on the radiation.

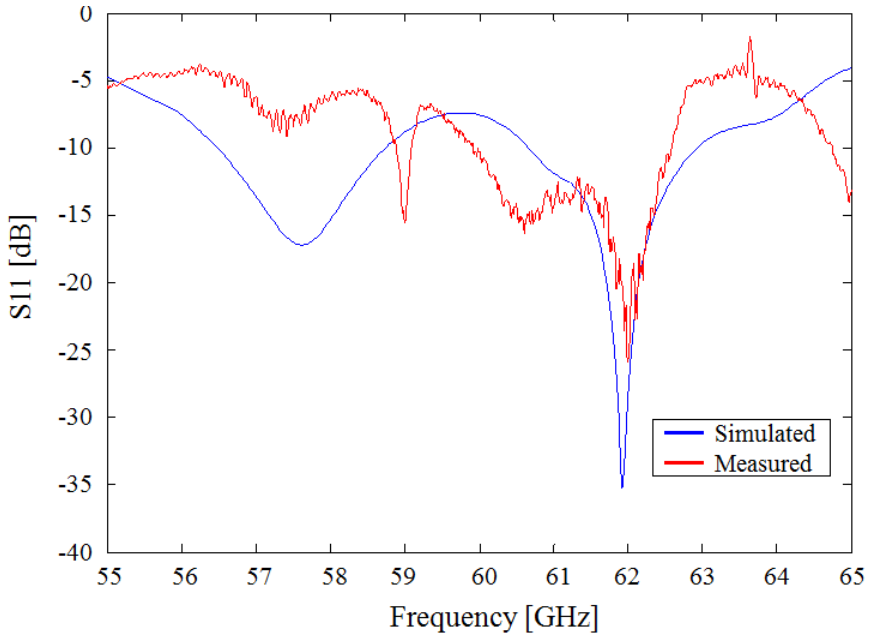

(a)

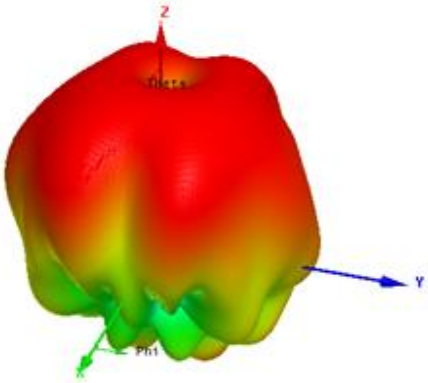

Height = 400 µm

(b)

Figure 23. (a) Measured S_{11} vs frequency for 400 µm Si height; (b) 3D Radiation Pattern for 400 µm Si height at 62 GHz.

3.3 Hybrid Silicon-Organic Packaged Antennas Using a Low-Cost Bonding Technique

To minimize surface wave effects from high dielectric constant substrates, a hybrid integration of silicon and organic substrates may be used. This enables separate selection of RF and electronics substrates. Having this type of integration allows combining the CMOS Si electronics with Multi-Layered Organics (MLO), which yield high performing antennas. Both RO3003™ and LCP prove to be excellent choices as organic RF substrates due to their electrical properties (ε_r=3, tan δ=0.002) and relatively low fabrication costs [24,29]. The latter has been shown to have great performance in packaging of RF devices [58] and it requires low processing temperatures (less than 290°C), which makes it ideal for multi-layered designs. Antenna-in-Packages at mm-wave frequencies are mainly integrated through wirebonds [6] or flip-chip bonding [7]. However, unlike what is traditionally done, herein, the bonding is secured by melting a non-conductive film (NCF) layer. This has the advantages of simplicity and reducing costs when using organic substrates. This work, presented at the 2012 International Microwave Symposium [51], focuses on a simple silicon-organic hybrid packaged antenna that is low cost, provides easy integration and exhibits good performance.

FOUR-ELEMENT ANTENNA ARRAY

With the interest of covering 10% bandwidth with a high gain, two 4-element dipole arrays were designed at 60 and 80 GHz. These followed the highly directive dipole in [59]. The multi-layered design has the advantage of an embedded feedline, which avoids losses

and spurious radiation, particularly at higher frequencies. The complete packaged arrays are 12 mm x 10 mm in size, as depicted in Figure 24.

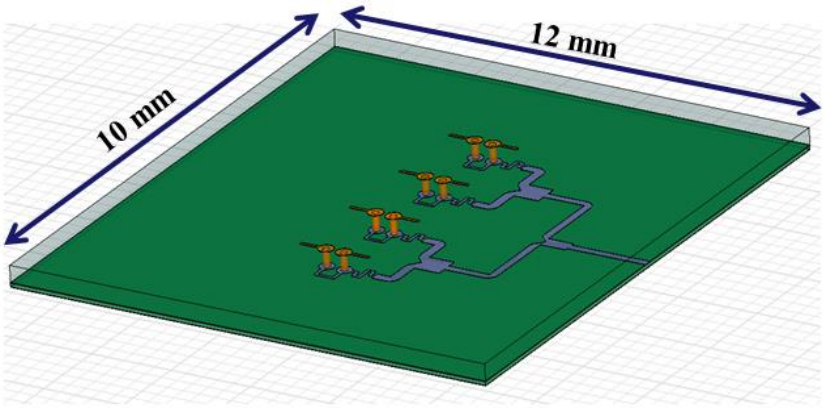

Figure 24. 3D-view of four-element dipole array.

To attain high gain and a broad bandwidth, a substrate with thick height and low dielectric constant are required. Similar to LCP but available in thicker heights, Rogers RO3003™ was chosen as the antenna substrate. A thinner thickness is needed for the feed network substrate as it yields better RF performance. Since ULTRALAM® 3850 (LCP) is available in 1, 2 and 4 mil, it was used. The feed includes a microstrip corporate feed network to evenly feed the antenna, and various quarter-wavelength transformers for impedance matching. For optimum results, the total height of each packaged antenna (including the feed substrate) is roughly a quarter of a wavelength. This implies using a stack-up combination of 20 mil RO3003™ and 4 mil LCP for the 60 GHz design, and 15 mil RO3003™ and 2 mil LCP for the 80 GHz design. The antenna was then flip-chip bonded onto the silicon substrate using a very simple technique where the NCF layer mechanically secures the bumps. An aluminum coplanar line was designed on the 400 µm

thick silicon substrate, which could contain CMOS circuits. The complete area of the Si is 16 mm x 10 mm. The first BCB layer on top of the Si supports interconnects and the second acts as passivation layer. After the coplanar line was optimized, the transition going from ML2 through IL2 to the silicon substrate was designed. This one included a filled via through the LCP substrate, whose diameter has a one- to-one ratio with the substrate height. Transition details for the via interconnect with the gold bump and silicon substrate are illustrated in Figure 25.

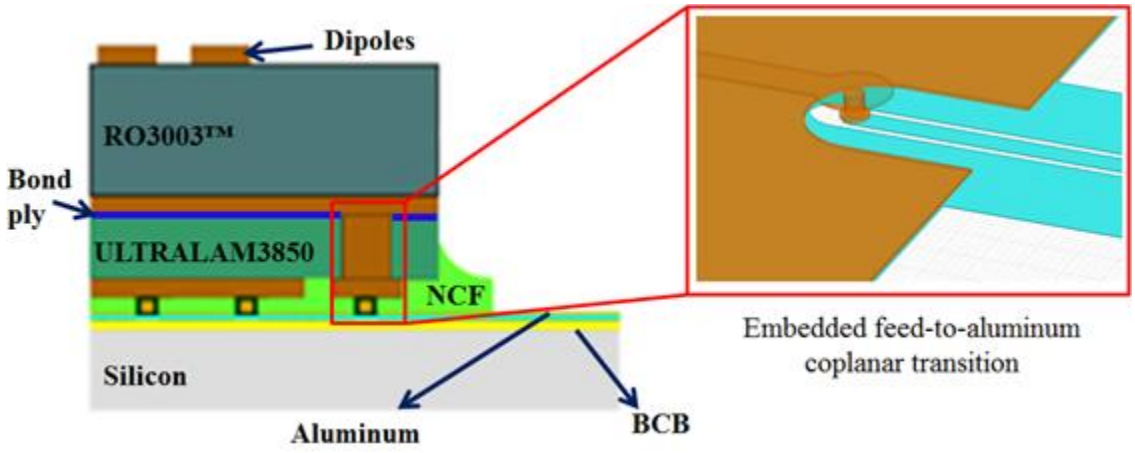

Figure 25. Hybrid organic-silicon cross-section with gold bumps and via transition.

FABRICATION AND BONDING PROCESS DETAILS

Several hundred 50 μm x 50 μm openings were patterned on the BCB layer (Figure 26), in order to access the CPW aluminum ground and keep good connection between the metal layers. These served as the landing pads for the gold bumps. To assist the bonding process, a non-conductive film (NCF) was used.

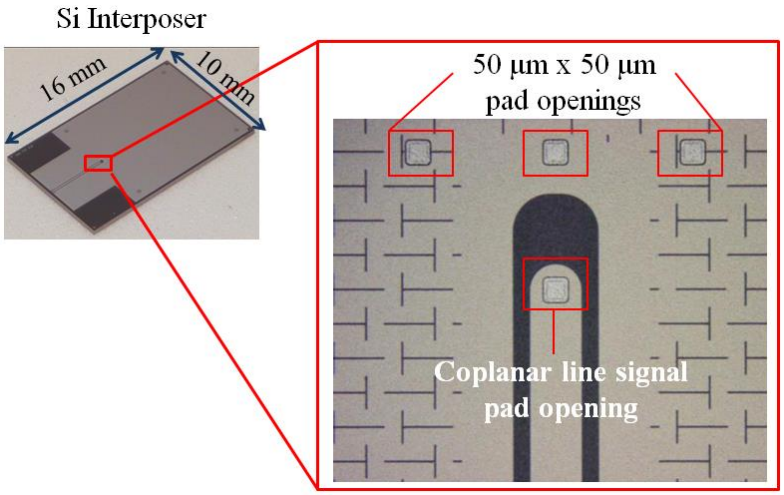

Figure 26. Coplanar line on silicon interposer with pad openings for gold bumps.

After gold bumps were placed on the LCP chip, it was flip-chip bonded onto the silicon substrate. Instead of melting the bumps, the NCF was heated under pressure to secure the bonding. The complete process flow for the bonding technique is shown in Figure 27.

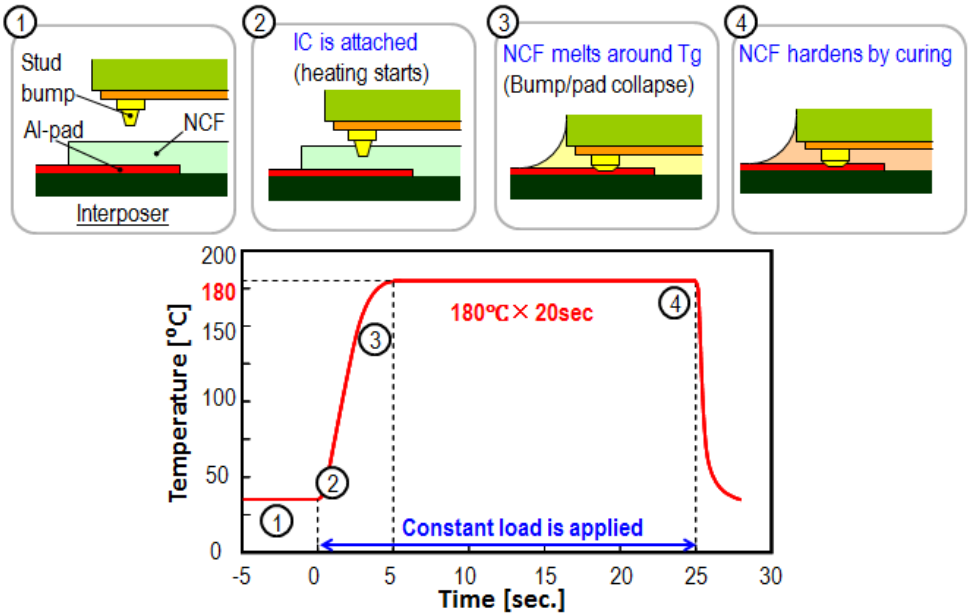

Figure 27. NCF assisted bonding process flow.

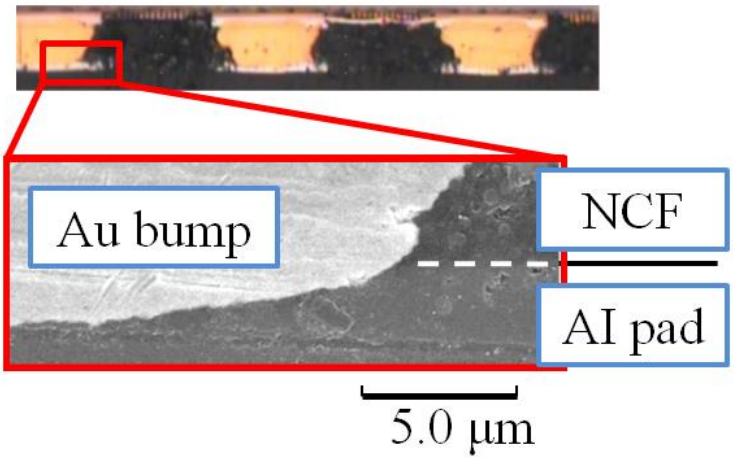

(a)

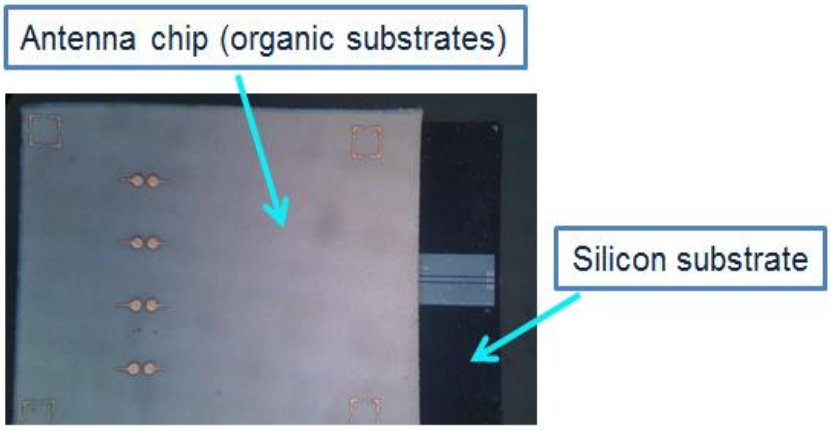

(b)

Figure 28. (a) SEM image of gold bump and aluminum-NCF interface; (b) Photo of the fabricated organic antenna flip-chip bonded to the silicon substrate.

Figure 28(a) shows the gold stud-bump drove wedge into the aluminum pad, confirming the successful fabrication of an ohmic contact. The complete bonded organic-silicon hybrid structure can be seen in Figure 28(b).

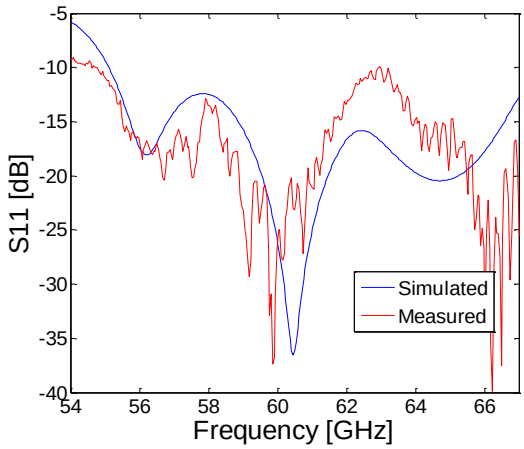

(a)

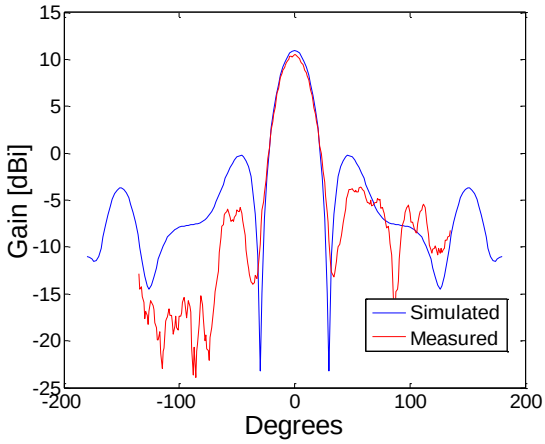

(b)

Figure 29. Measured results: (a) S_{11} vs Frequency for 60 GHz array; (b) H-plane patterns for 60 GHz array.

The bandwidth of the 60 GHz design extends roughly from 55 to 67 GHz. This plot is seen in Figure 29(a). The measured gain was stable from 55 to 65 GHz, with a maximum value of ~10.5 dBi. A comparison of the measured and simulated patterns is shown in

Figure 29(b) and it can be seen that there is good agreement between the simulated and measured results. The bandwidth of the 80 GHz design, as seen in Figure 30(a), extends from 71 to 88 GHz. In Figure 30(b) we see the gain for this design peaking at 10 dBi. For both arrays, the patterns are stable within desired the bandwidth.

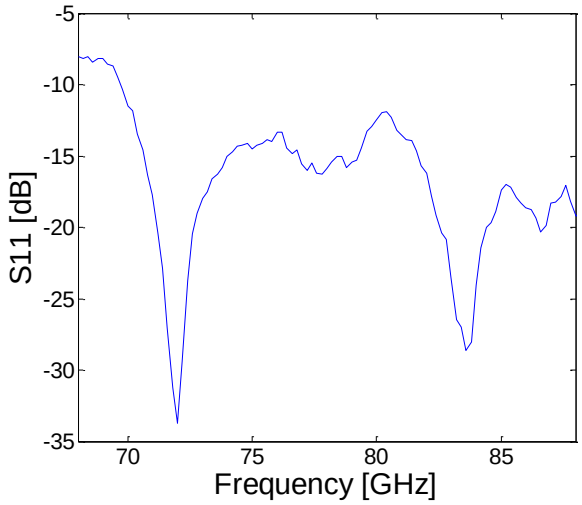

(a)

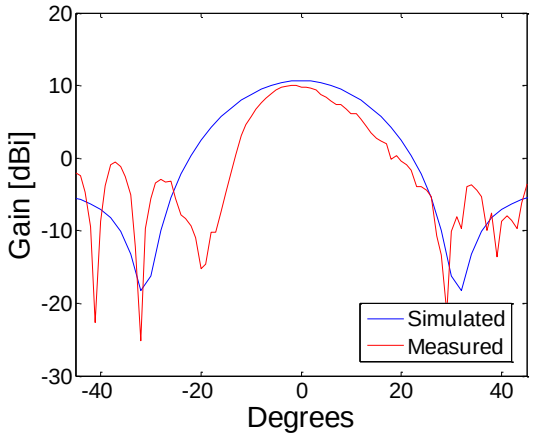

(b)

Figure 30. Measured results: (a) S_{11} vs Frequency for 80 GHz array; (b) H-plane patterns for 80GHz array.

3.4 Dual Packaged Organic Dipoles

Now that the bonding technique proved successful, both dipole arrays need to be packaged together. This portion focuses on the design of the 4-element dipole arrays as they are packaged together on organic substrates, at 57 and 80 GHz respectively. The feed network has been altered to include a T-junction for the arrays to be fed together, which serves to simulate both arrays operating simultaneously. Figure 31 shows a 3D-view of the layers and the changes made to the stack-up. This one now uses 15 mil thick RO3003™ as the antenna substrate and 2 mil ULTRALAM® 3850 as the feed network's substrate. Also, for measurement ease, the design now has the feed on the bottom layer. This allows probing without making additional openings and has the advantage of providing a cleaner pattern, because the ground is now in between the dipoles and feed. Findings were published at the 2013 International Microwave Symposium [60].

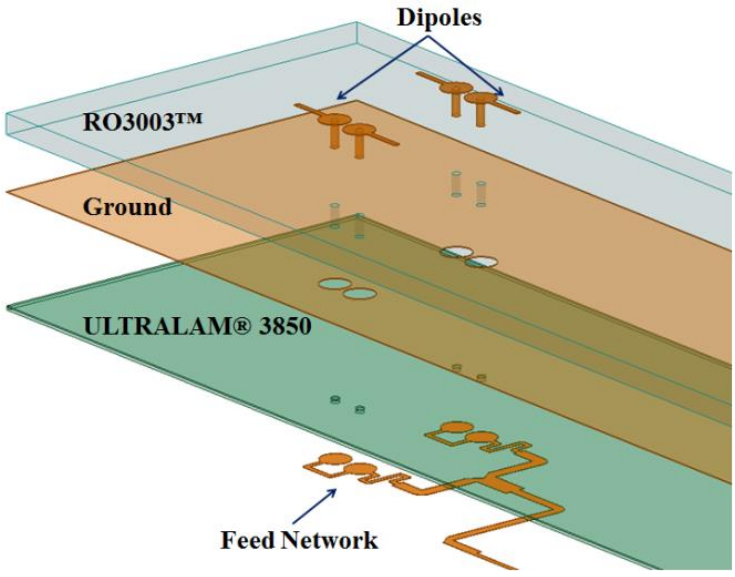

Figure 31. 3D-view of array MLO stack-up.

The feed network includes a microstrip corporate feed to evenly feed the antennas, quarter-wavelength transformers for impedance matching and a microstrip to coplanar transition for probing. The axes of the two arrays that connect to the T-junction were oriented at different angles with respect to each other in order to evaluate their performance. As we seek to reduce any interference, a 45º rotation on both designs lessens the losses suffered in the radiation patterns. Stand-alone designs were also fabricated to compare their radiation performance with the dual frequency packaged arrays. An individual dipole array can be seen in Figure 32(a) and a top-view of the complete packaged antennas in Figure 32(b). The dipole orientation was chosen based on full-wave analysis to minimize any antenna interaction. As it is shown, the two arrays differ by 90 degrees in their orientation.

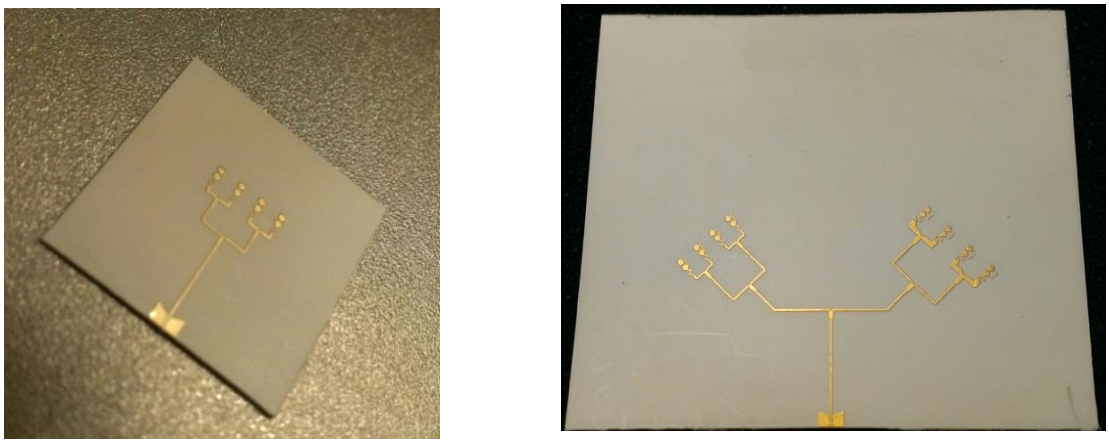

(a) (b)

Figure 32. (a) Packaged dipole array in MLO; (b) Top-view of dipole arrays with T-junction.

The packaged antennas were probed using a 250 µm GSG GGB Pico probe. The bandwidth of the 57 GHz (Figure 33(a)), extends from 54 to 61 GHz (~12%). For the 80 GHz design (Figure 33(b)) it extends from 76 to 85 GHz (~11%). The measured gain H-plane patterns are found in Figure 34.

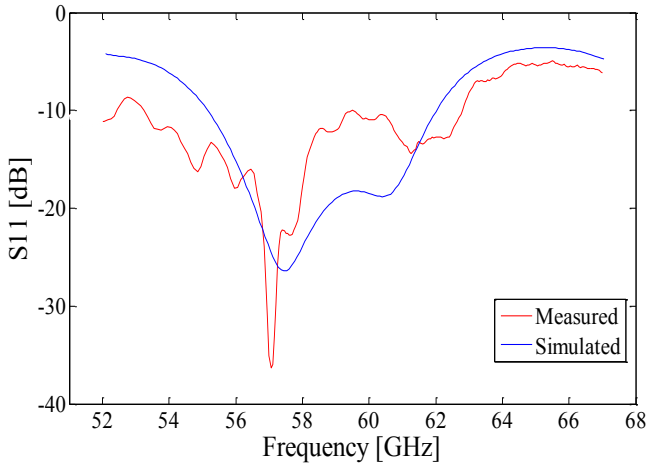

(a)

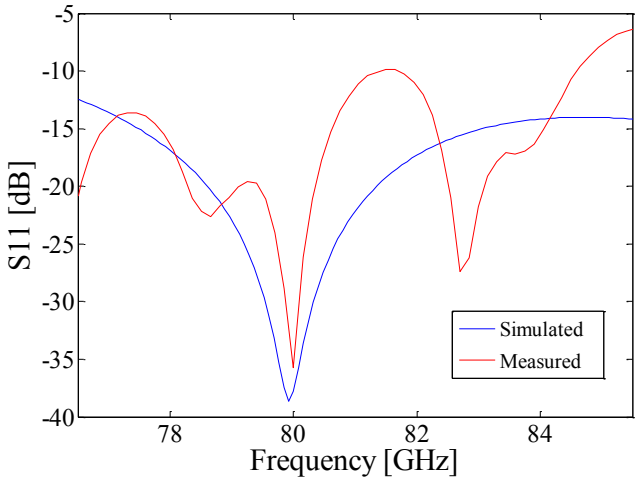

(b)

Figure 33. Measured results: S_{11} vs. Frequency for (a) 57 GHz array and (b) 80 GHz array.

The stand-alone 57GHz design without the T-junction achieves a maximum gain of almost 10 dBi (Figure 34(a)). This value drops slightly once we have the T-junction with both antennas (~9 dBi). Figure 34(b) shows the measured pattern of the 80 GHz designs, which peaks close to ~10 dBi. Here, we also observe the effect of the nearby 57 GHz (found on the right, positive degrees), which raises the side lobe level.

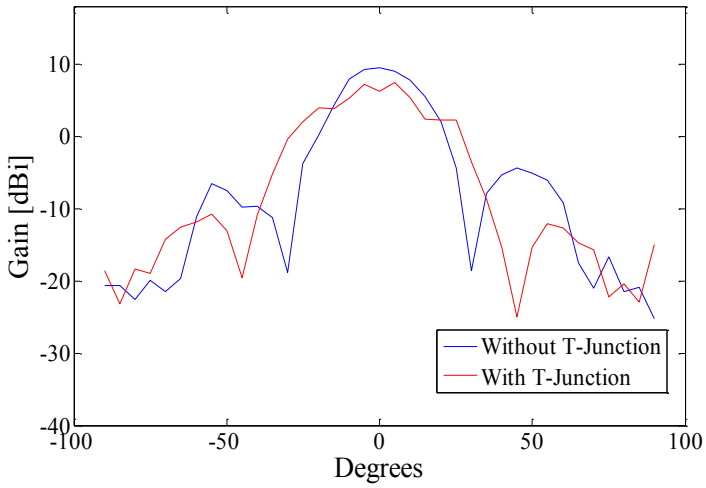

(a)

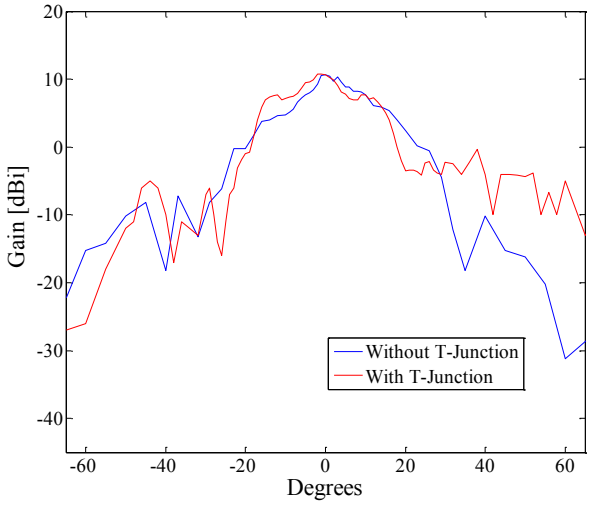

(b)

Figure 34. Measured H-plane patterns: (a) 57 GHz array and (b) 80 GHz array.

CHAPTER 4:

FULL SYSTEM INTEGRATION

4.1 Orientation Study to Reduce Proximity Effect on Antenna Radiation

While being simultaneously excited, evidence of good performance for both antenna array designs was presented in the previous section. The 45 degree orientation used aided in minimizing any proximity effects seen by the antennas. These results serve as a stepping stone to enabling the promising prospect of simultaneous communications. In this section, a closer look at the different orientations is presented. For the first time to the best of the author's knowledge, a study of different antenna orientations and how these affect the E- and H-plane radiation patterns of two printed antennas packaged together in multilayer organic (MLO) substrates at 57 and 80 GHz for high-speed half- or full-duplex communication systems was done. The complete study was published in IET's Microwaves, Antennas and Propagation Journal [28].

In this study, the same two 4-element dipole arrays previously discussed were used. The multilayer organic stack-up is seen in Figure 31. The overall size of the integrated arrays with T-junction is 30 mm x 40 mm. A 3D-view of the arrays with T-junction is shown in Figure 35(a). In the experiment, the two arrays are oriented at different angles with respect to a vertical axis. The three configurations under study are 0°, 45° and 90° (Figure 35(b)). Each configuration was simulated using Ansoft's High Frequency Structure Simulator (HFSS).

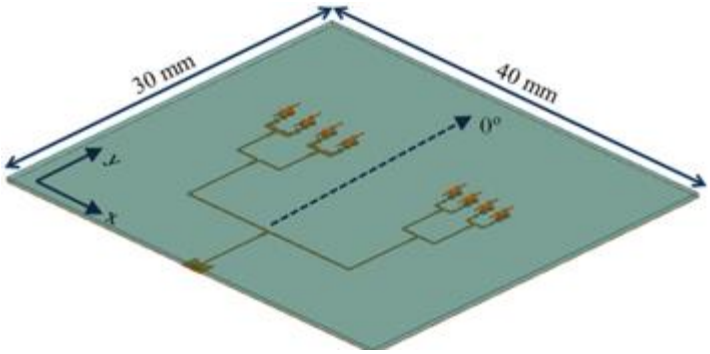

(a)

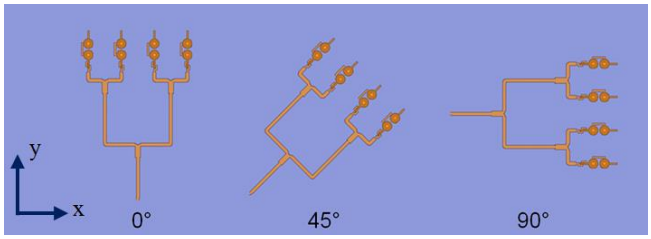

(b)

Figure 35. (a) 0° Configuration connected through T-junction; (b) Orientations under study.

FABRICATED DESIGNS

The antennas were fabricated using standard PCB fabrication processes. The backside of the 15 mil RO3003™ antenna substrate (ground openings for vias) was patterned through photolithography. Then, the feed and antenna substrates were laminated together using a 1mil RO3908® bond ply. The thru vias connecting the dipoles to the feed were then drilled and plated. Finally, the dipoles and feed lines were patterned. The fabricated design configurations are shown in Figure 36. A distance of 10 mm was chosen between the designs. This corresponds to approximately $2\lambda_0$ at 57 GHz, or $2.67\lambda_0$ at 80 GHz.

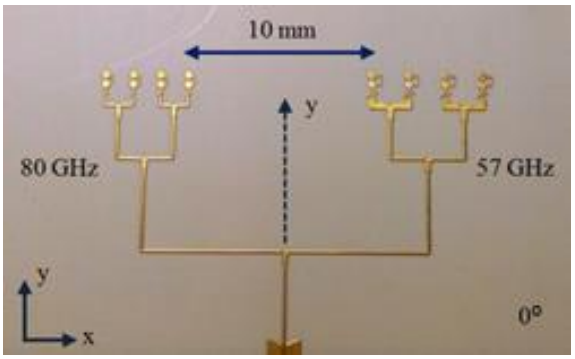

(a)

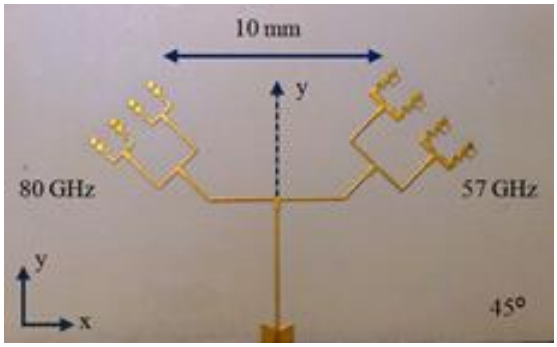

(b)

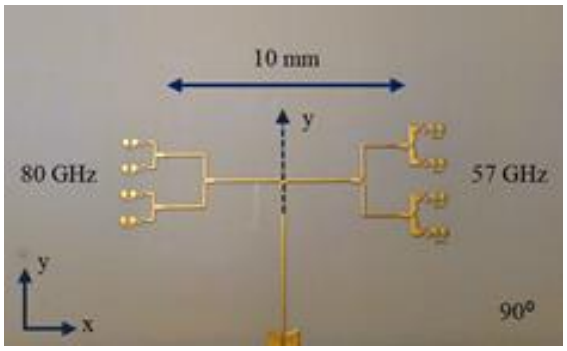

(c)

Figure 36. Fabricated arrays with T-Junctions and varying orientations: (a) 0° orientation, (b) 45° orientation and (c) 90° orientation.

MEASUREMENTS AND RESULTS - ORIENTATION VARIATION EXPERIMENT

The antennas were measured using a 250 μm pitch Picoprobe held by an Alessi probe holder. Measurements were performed on a specialized probe station that consists of a Styrofoam stage that the Antenna Under Test (AUT) sits on and a standard gain horn receiving antenna held on an arm that rotates around the AUT with a radius of 30 to 60 cm. The arm rotates from 0º to 180º. The system is within an area shielded with microwave absorbing material in an anechoic chamber. Figure 37 illustrates this setup.

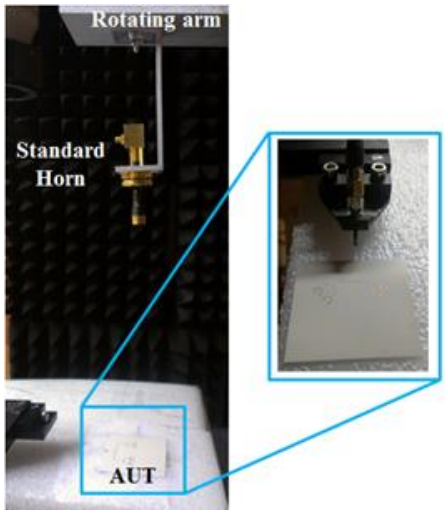

Figure 37. Radiation patterns measurement setup.

For the 57 GHz measurements, an Agilent vector network analyzer is used, with a Quinstar Low Noise Amplifier on the receiving side to increase dynamic range. On the transmitting side of the 80 GHz measurements, the RF signal is generated by an Agilent signal generator and then up converted by a source module (83558A). At the receive antenna, the RF signal is first amplified with the LNA and then down converted to the IF frequency. A signal analyzer is used to measure the power of the received signal. The gain is measured using the substitution method with a 25 dBi gain horn as the "known" antenna

for the 57 GHz measurements, and a 16 dBi gain horn for the 80 GHz measurements. The standard horn was rotated to match polarization for all E- and H-plane measurements. Results for the 0° configuration at 57 GHz are shown in Figure 38. The scales provide 360º in polar format with gain values in dBi. The main lobe in the H-plane has some pronounced ripples due to the presence of the neighboring antenna. The E-plane is cleaner and only has ripples around the edges mainly due to the setup and probe. The gain peaks close to 10 dBi.

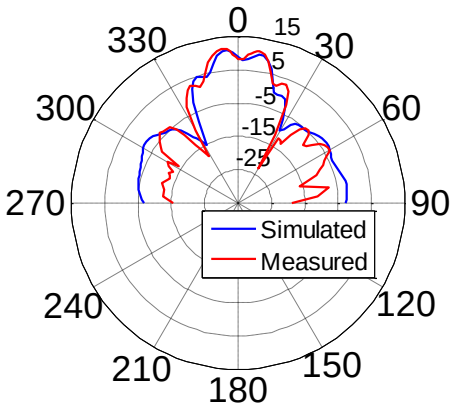

(a)

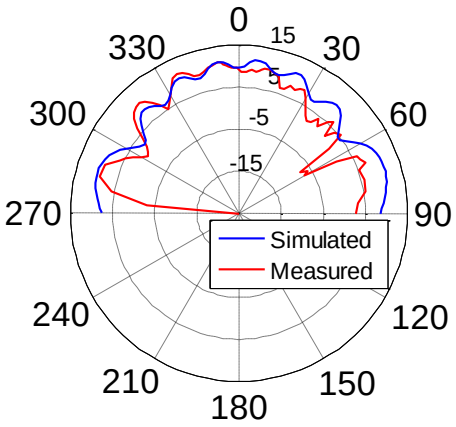

(b)

Figure 38. Measured patterns for 57 GHz - 0^0 configuration: (a) H-plane and (b) E-plane.

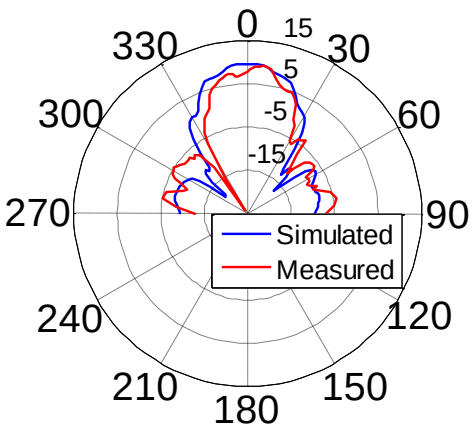

(a)

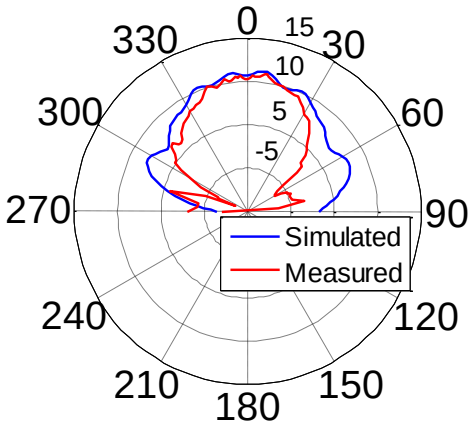

(b)

Figure 39. Measured radiation patterns for 57 GHz array - 45^0 configuration: (a) H-Plane and (b) E-Plane.

Results for the 45° configuration at 57 GHz are shown in Figure 39. While the H-plane has are some ripples in the main lobe, these are reduced compared to Figure 38(a). E-Plane plot is also overall smoother.

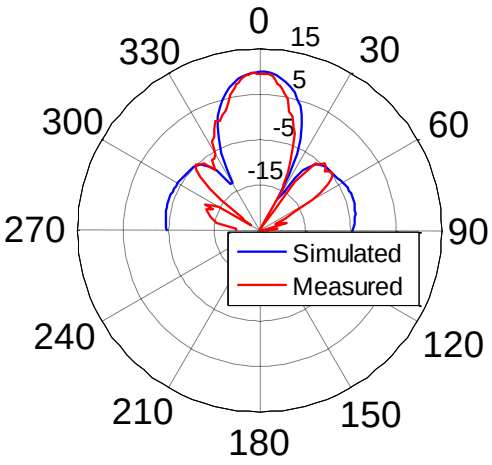

(a)

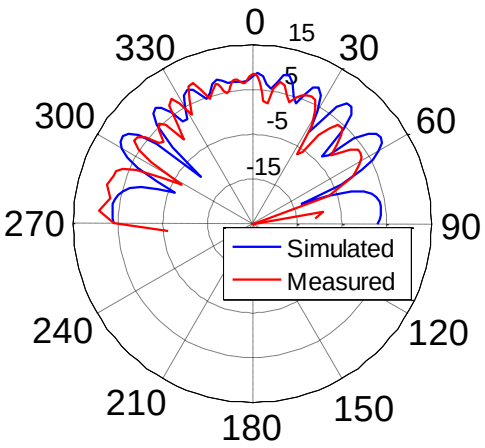

(b)

Figure 40. Measured radiation patterns for 57 GHz array - 90^0 configuration: (a) H-Plane and (b) E-Plane.

Figure 40 shows results for the final configuration at 57 GHz. As the designs are now on the same horizontal line parallel to the E-Plane, results should thus showcase the effect of seeing both designs in that plane. Sweeping the H-plane, however, only one design is seen and this pattern cut should be significantly better. Figure 40(a) shows exactly that; a mainly ripple-free and smooth H-plane cut. The E-plane has substantial ripples throughout the entire plot. The maximum gain peaks around 9.95 dBi.

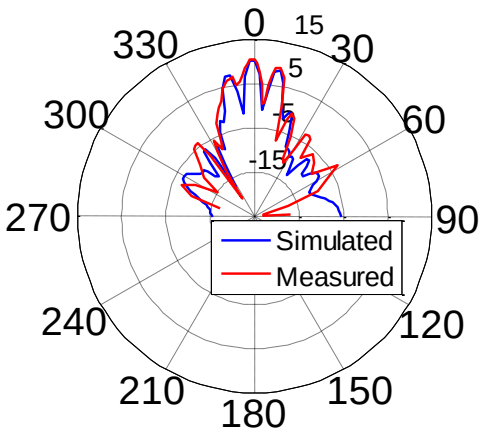

(a)

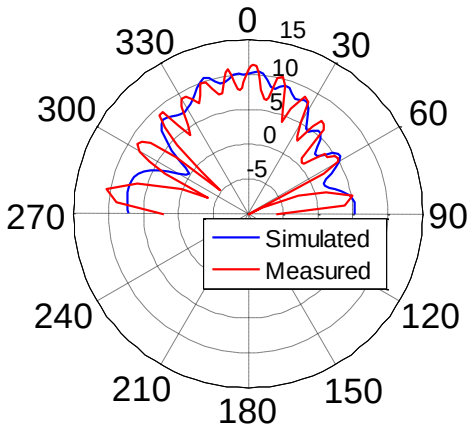

(b)

Figure 41. Measured radiation patterns for 80 GHz array - 0^0 configuration: (a) H-Plane and (b) E-Plane.

Similar to what is seen at 57 GHz in Figure 38, the results for the 0° configuration at 80 GHz (found in Figure 41), show significant ripples in the main lobe for the H-plane pattern cut. The E-plane has some ripples as well, but not as pronounced. The gain peaks close to 10.5 dBi.

The 45° configuration results at 80 GHz can be seen in Figure 42. Significant improvement in the ripples both in the H- and E-plane cuts is seen, when compared to the previous 0° configuration. The maximum gain is almost 10 dBi.

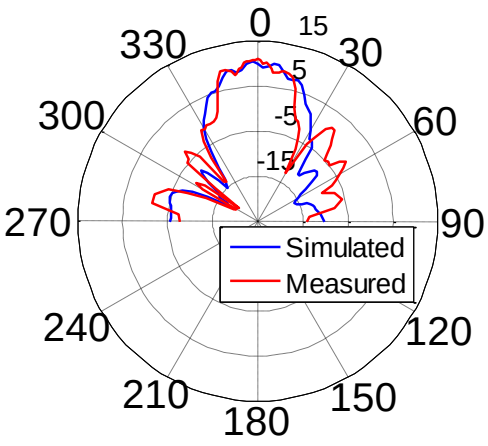

(a)

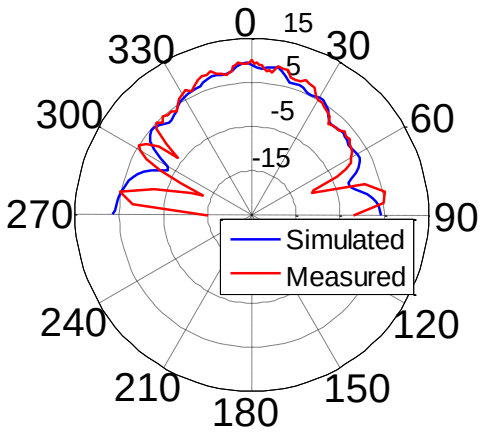

(b)

Figure 42. Measured radiation patterns for 80 GHz array - 45^0 configuration: (a) H-Plane and (b) E-Plane.

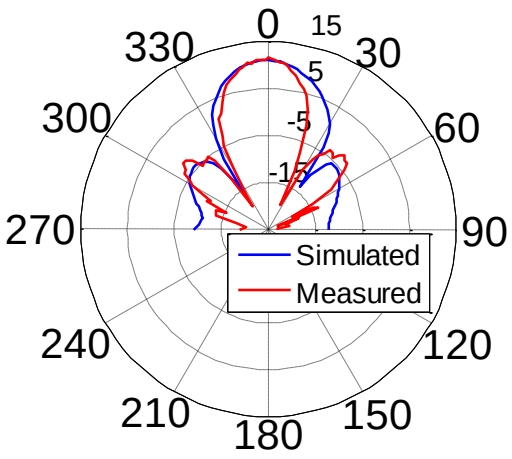

(a)

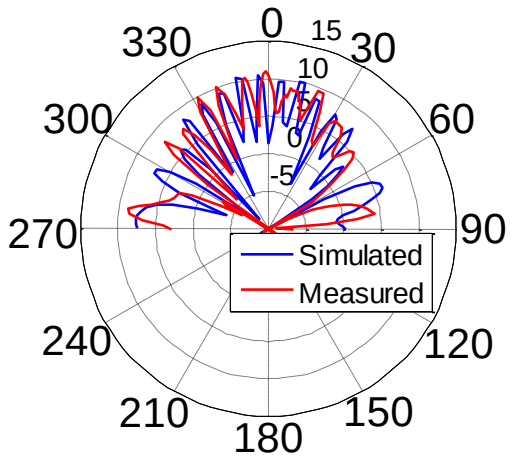

(b)

Figure 43. Measured radiation patterns for 80 GHz array - 90^0 configuration: (a) H-Plane and (b) E-Plane.

The measured results for the 90° configuration at 80 GHz are found in Figure 43, where we see a completely ripple-free H-plane. The E-plane has severe ripples all throughout the plot. Both plots have a peak gain of ~10.1 dBi. Table 8 provides a summary of all the measured results for both the 57 and 80 GHz arrays for this portion of the study.

Table 8. Summary of radiation results of orientation study

Design	# of ripples (±60°)		Average level (dB)		Max Gain (dBi)	
	E	**H**	**E**	**H**	**E**	**H**
0° - 57 GHz	6	4	2.1	3.2	10.15	10.09
0° - 80 GHz	8	3	1.3	5.6	10.82	10.21
45° - 57 GHz	8	3	0.43	1.3	10.28	9.80
45° - 80 GHz	6	3	1.62	1.72	9.97	10.33
90° - 57 GHz	10	0	4.79	0	9.93	10.02
90° - 80 GHz	9	1	6.1	0.2	10.24	10.61

While one pattern cut was cleaner for each of the 0° and 90° configurations, this was at the cost of having the other cut suffer significant ripples. The 45° orientation presents the best compromise in the results, having good results for both pattern cuts. Incorporating these rules into dual packaged antennas will significantly improve their results, and, for those simultaneously excited, will guarantee better performance in high speed millimeter-wave wireless communication systems.

4.2 Distance variation experiment

To see what kind of effect adding additional spacing between the arrays will have on the 0^0 and 45^0 configurations, two designs were fabricated with an additional λ_0 at 57GHz, or $1.33\lambda_0$ at 80GHz, of extra feedline length. The additional length is along the y-axis for the 0^0 orientation, and diagonally for the 45^0, extending from start of the feedline to the where the design's T-junction splits. These configurations are shown in Figure 44.

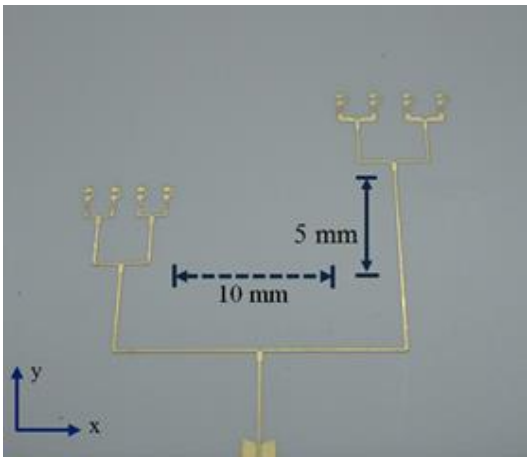

(a)

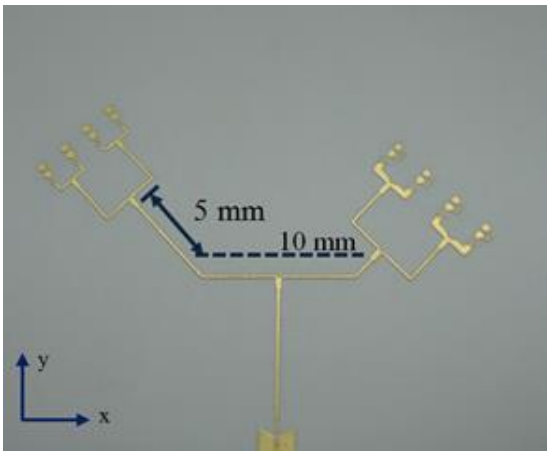

(b)

Figure 44. Arrays with additional spacing: (a) 0^0 configuration; (b) 45^0configuration.

57 GHz Measurements

The patterns at 57 GHz for the 0^0 configuration are found in Figure 45. Compared to what is seen without this additional spacing in Figure 27(a) and (b) for this configuration, the average ripples in the H-plane are reduced from 3 to 1.3 dB; and in the E-plane from 2.1 to 1.7 dB. Though these are overall smoother, they do possess about 0.5 dB less gain (~9.6 dBi), due to the additional 5 mm line length. This is expected from a longer line. At the same time, the change in $|S_{11}|$ is negligible for additional length.

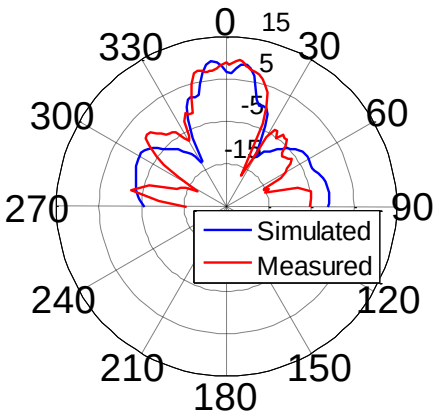

(a)

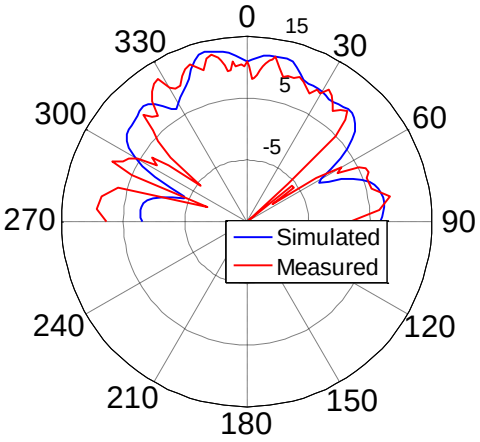

(b)

Figure 45. Measured radiation pattern cuts for the 57 GHz array - 0^0 configuration with additional spacing: (a) H-Plane; (b) E-Plane.

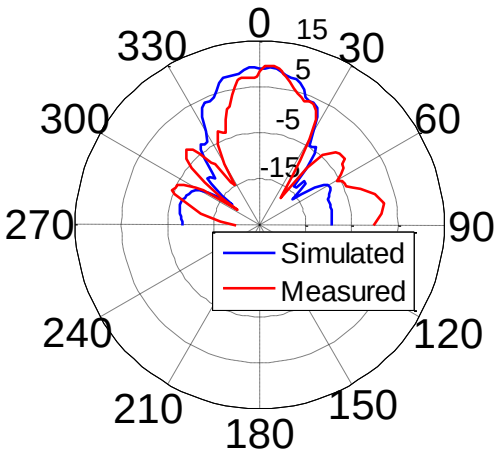

(a)

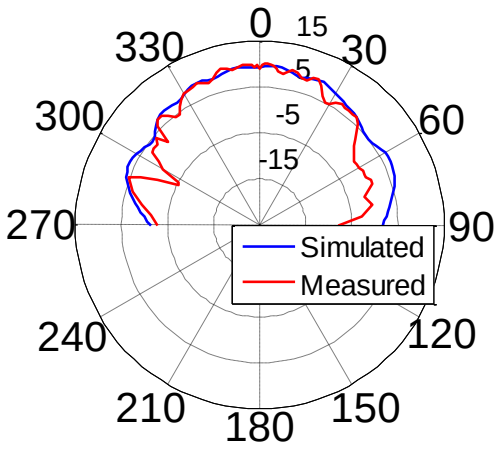

(b)

Figure 46. Measured radiation pattern cuts for the 57 GHz array - 45^0 configuration with additional spacing: (a) H-Plane; (b) E-Plane.

In Figure 46(a) and 46(b) we can see the measured patterns for the 45^0 configuration with the extra spacing (seen in Figure 44(b)). Compared to what is shown in Figure 39(a) and 39(b), there is no significant improvement in the amount of ripples in both plots. The gain in both plots dropped close to 0.4 dB (~9.5 dBi). Table 9 lists a complete summary of all measured data for 57 GHz designs.

Table 9. Data results' summary for 57 GHz array

Design	# of ripples (±60°)		Average level (dB)		Max Gain (dBi)	
	E	**H**	**E**	**H**	**E**	**H**
0° orientation	6	4	2.1	3.2	10.15	10.09
45° orientation	8	3	0.43	1.3	10.28	9.8
90° orientation	10	0	4.79	0	9.93	10.02
0°+ λ_0 spacing	7	2	1.7	1.3	9.6	9.71
45°+ λ_0 spacing	6	2	1.6	1.2	9.41	9.92

80 GHz Measurements

The measured H- and E-plane patterns at 80 GHz for the 0^0 configuration with additional spacing between the designs are found in Figure 47(a) and (b), respectively. For this configuration, the H-plane shows an overall reduction in the ripples of approximately 3 dB. However, while the E-plane's average ripple level stayed roughly the same (Figure 47(b)), the number of ripples was reduced from 8 to 4. The peak gain for both cuts in this configuration is around 9.8 dBi.

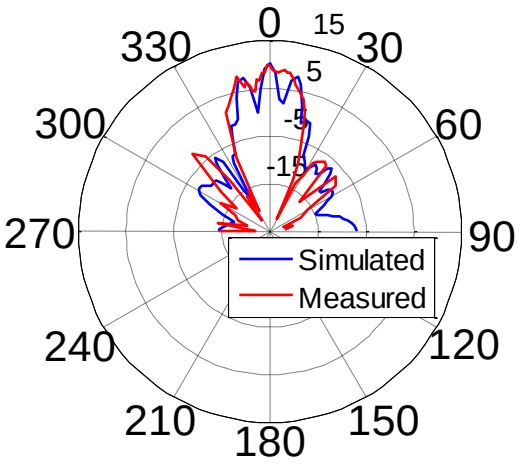

(a)

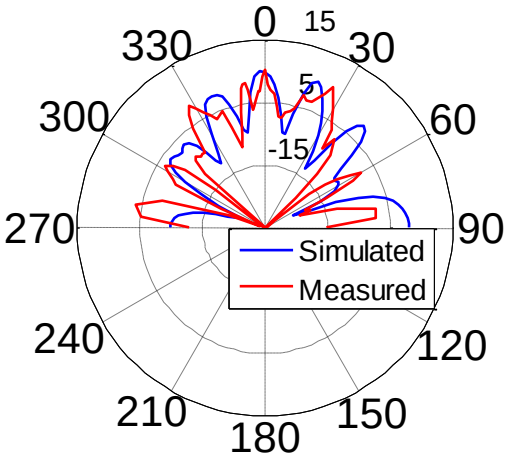

(b)

Figure 47. Measured radiation pattern cuts for the 80 GHz array - 0^0 configuration with additional spacing: (a) H-Plane; (b) E-Plane.

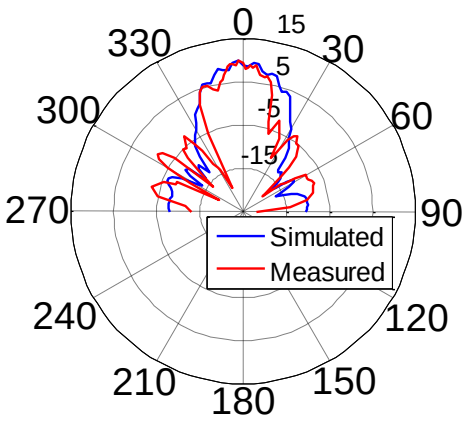

(a)

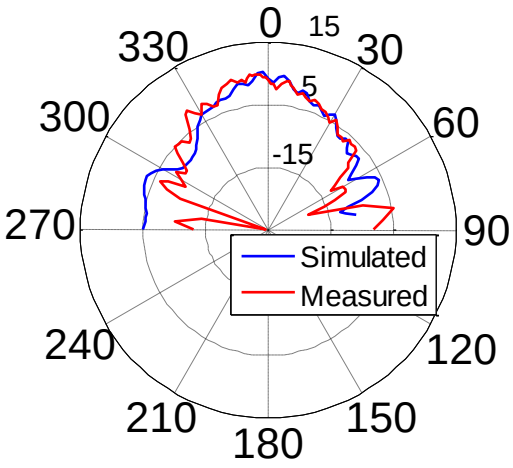

(b)

Figure 48. Measured radiation pattern cuts for the 80 GHz array 45^0 configuration with additional spacing: *(*a) H-Plane; (b) E-Plane.

Finally, the 80 GHz patterns for the 45^0 configuration with additional spacing are found in Figure 48. In both patterns, a very slight reduction in the amount of ripples and their level is seen (~0.2 dB). Once again, the additional line length reduced the gain by 0.4 dBi. A summary of the data for all measured 80 GHz designs is found in Table 10.

Table 10. Data results' summary for 80 GHz array

Design	# of ripples (±60°)		Average level (dB)		Max Gain (dBi)	
	E	**H**	**E**	**H**	**E**	**H**
0°	8	3	1.3	5.6	10.82	10.21
45°	6	3	1.62	1.72	9.97	10.33
90°	9	1	6.1	0.2	10.24	10.61
0° + 1.33λ_0 spacing	4	2	1.6	2.61	9.74	9.92
45° + 1.33λ_0 spacing	5	2	1.6	1.3	9.48	9.89

RECOMMENDED GUIDELINES

The following points summarize the performed experiments and should be used as guidelines when integrating highly compact dual frequency antenna designs in-package at mm-wave frequencies.

- The best orientation to minimize ripple level and amount in both pattern cuts is at a 45º orientation, with respect to the axis (orthogonal array orientation).

- If space allows and gain can afford an average loss of ~ 0.5 dB, an extra spacing of λ_0 will help further smooth the patterns by reducing the number of ripples (4 in the best case) or their level (1 dB on average).

- For a given application, if the quality of one pattern cut is more important than the other, the 0º or 90º configurations can provide good results.

- For simultaneous excitation at mm-wave, it is sufficient to have the antennas at a 45º orientation to have good performance and keep the package size small.

4.2 RF CMOS Integration

In [16] a plastic waveguide is used as a board-to-board interconnect. The RF CMOS chips used in the system possess two baseband inputs and two separate outputs, for two different frequencies. This means they have one output set for 57 GHz and one for 80 GHz, as seen in Figure 49. These connect to two Quasi-Yagi antennas that act as couplers. In their system, a full-duplex transmission through the plastic waveguide achieves a total data rate of 25 Gb/s, for a distance of 120 mm.

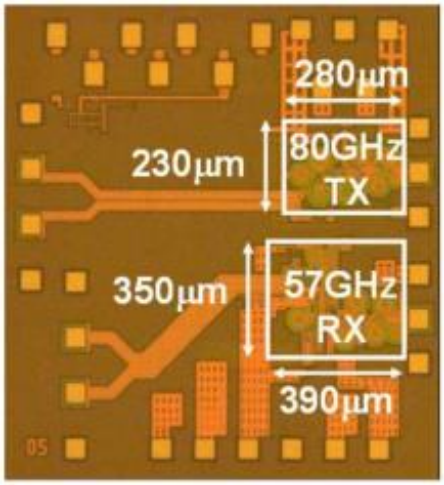

Figure 49. RF CMOS chips with two separate outputs [16].

Similar to what was achieved in [16], we seek a full-duplex system based on wireless transmission and fully packaged on multilayer organic substrates. Also, as opposed to the double output pads found in [15,16], the chip used has a single output that may be used for a dual-design (Figure 50). This will allow simultaneous excitation of two designs. The output will transition to a T-junction network that feeds the two different dipole arrays, at 57 and 80 GHz respectively. To the author's knowledge, this is the first

full-duplex system integrated on organic substrates to demonstrate simultaneous capabilities at millimeter-wave frequencies.

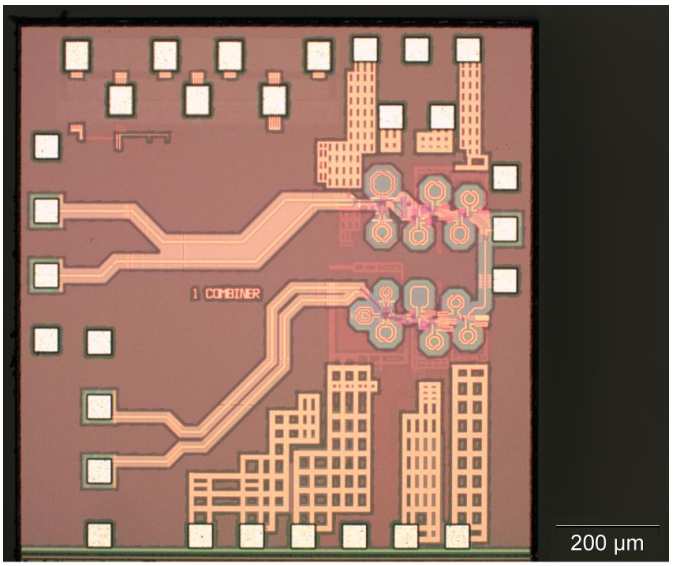

(a)

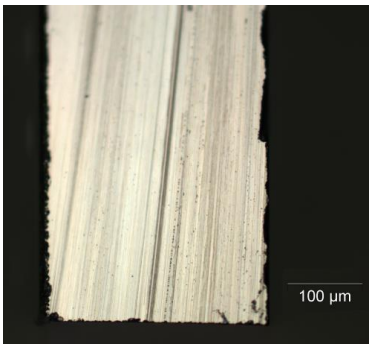

(b)

Figure 50. RF CMOS Tx chip: (a) top-view; (b) cross-section.

The studied four-element dipole arrays will be incorporated with the RF CMOS chip to create the full-duplex system. The best array orientation discussed in the previous section of this chapter will be used in the package. The complete integration requires the

three-layered MLO board used for the arrays to accommodate the routing paths, component pads and grounding for the chip. Details of the layers are shown in Table 11.

Table 11. Layer details for complete chip integration

Layer Name	Description	Material	Height
ML1	Feed, pads and routing lines	Copper	9 µm
IL1	Feed substrate	ULTRALAM3850®	2 mil
BP	Bond ply	ULTRALAM3908®	1 mil
ML2	Ground	Copper	17 µm
IL2	Antenna substrate	RO3003®	15 mil
ML3	Dipole array and routing lines	Copper	17 µm

INTERCONNECT PLANNING: WIREBOND VS FLIP-CHIP

Wirebonds have been successfully demonstrated to integrate systems at higher frequencies. However, the added inductance needs to be corrected and a compensation network is required to guarantee good performance. This network does not only add complexity to the design, but also narrows the bandwidth. Since the wireless transmission in [15] focused only one way around 60 GHz, wirebonds were used. For our full-duplex system, a broader bandwidth is required (50 to 90 GHz). Thus, wirebonding is not a suitable solution. Flip-chip bonding enables the broadband capabilities we need, while providing a good package for our board. However, careful planning needs to be done to our feedline

and routing layer (ML1, Table 11) to properly accommodate the pad sizes and transitions, without affecting our antenna performance. We will examine these in the next section.

MULTI-LAYER ORGANIC LAYERS: PLANNING AND DISTRIBUTION

The RF CMOS chip used, seen in Figure 50, has an area of 1000 µm x 1000 µm (with a 300 µm thickness. It is comprised of 29 pads. These include two differential baseband inputs for 57 and 80 GHz, found at the right side of the chip. There is one GSG RF output (for either 57 or 80 GHz), at the left side of the chip. For these RF pads, we needed to design 50 ohm lines on the first layer of the multi-layer organic stack-up (ML1). All the details of the stack-up distribution are described in Table 11. The first metal layer (ML1) sits on a 2 mil ULTRALAM3850® substrate (feed network substrate, for the dipole arrays). Figure 51 shows a top view of this metal layer.

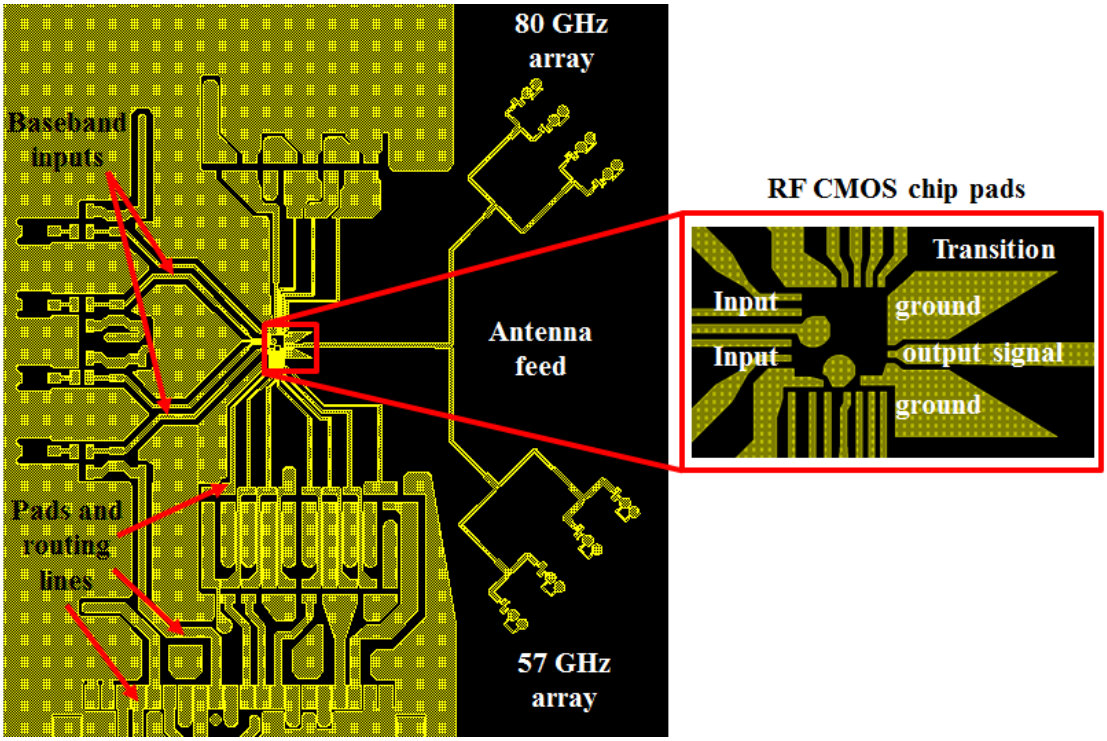

Figure 51. ML1 top-view: complete feed network, routing lines and pads.

ML1 possesses the majority of the routing lines to power the chip and connect all the corresponding elements. The elements consist of a combination of capacitors, inductors and resistors. It also has the differential 50 ohm lines for the baseband inputs (highlighted in Figure 51) and the feed network for the dipole array designs. The baseband inputs are around 3 GHz, and are later up-converted inside the chip to the desired frequencies. As with the previous antenna designs, the full feed network includes: series inductors and quarter-wave transformers for impedance matching, baluns for balanced to unbalanced output, and microstrip to coplanar transitions. These transitions also take into account the size of the pads where the gold bumps will be placed to flip-chip bond the chip onto the multi-layer stack-up. This is extremely important as the size and spacing of the pads need to perfectly align for bonding, while keeping losses minimal for the RF transitions involved. As was the case in Chapter 3.3, pads in layer were done to allow an area of about 50 µm x 50 µm for the gold bumps.

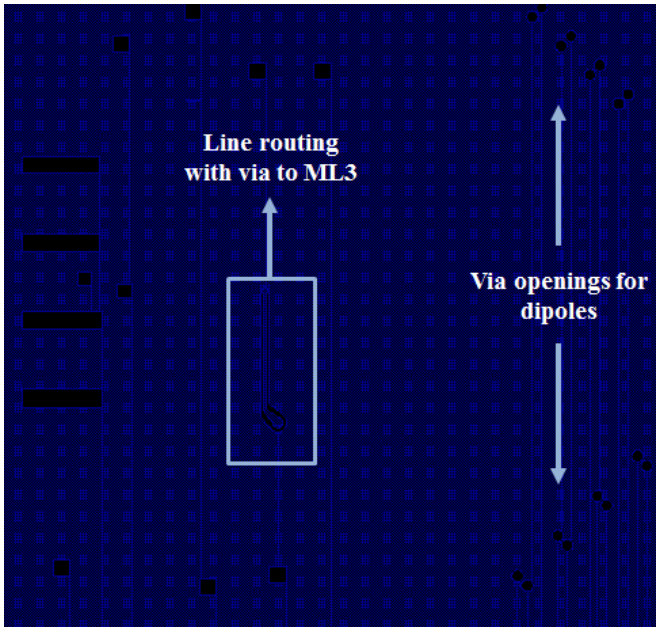

Figure 52. Metal layer 2 (ML2) top-view: RF ground and routing lines.

The second metal layer (ML2, Figure 52) serves as the main ground for the organic package, CMOS chip and antenna designs. It is the bottom metal of the 15 mil RO3003® antenna substrate. This one has several openings throughout that allow via connections from the first metal layer to the second and third metal layers. Amongst these connections there are some additional routing lines and the feed network to dipole vias. The third and last metal layer (ML3) has all the dipole array elements, some routing lines and grounding paths. The metal layer is distanced and tapered from the arrays to avoid negatively affecting their radiation patterns. Details on the last layer are found in Figure 53.

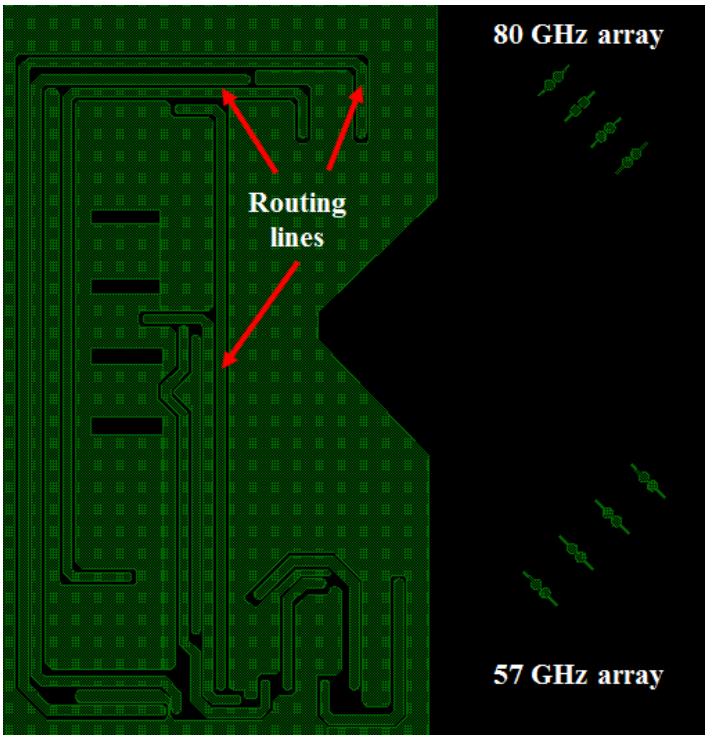

Figure 53. Metal layer 3 (ML3) top-view: dipole arrays and routing lines.

Results for the final fabricated packages are found in Figure 54. The figure shows a top-view of ML1 and ML3, and a detailed view of the transition to the dipole arrays.

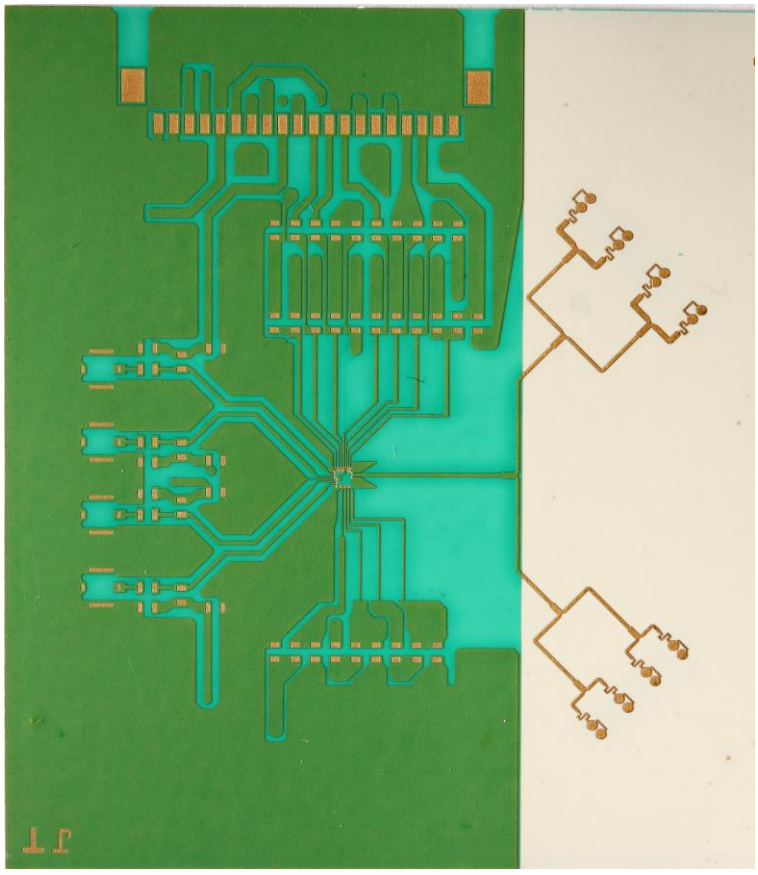

(a)

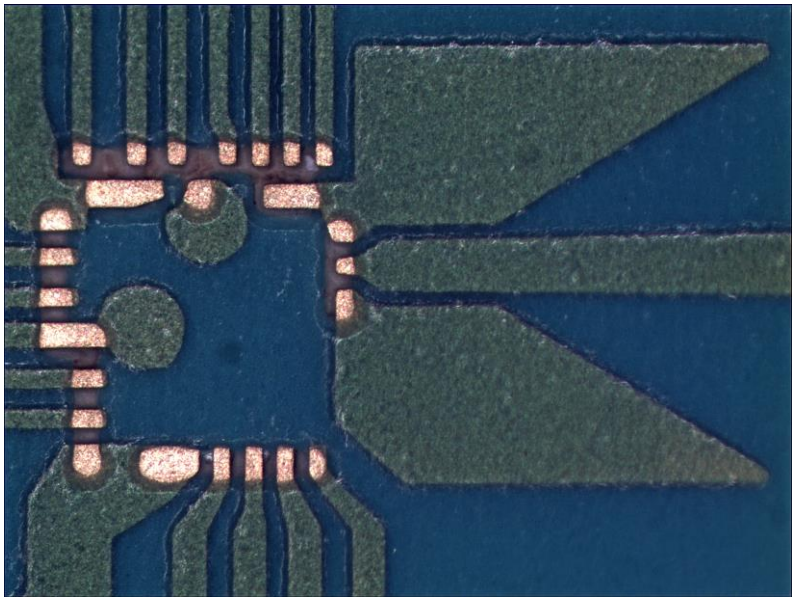

(b)

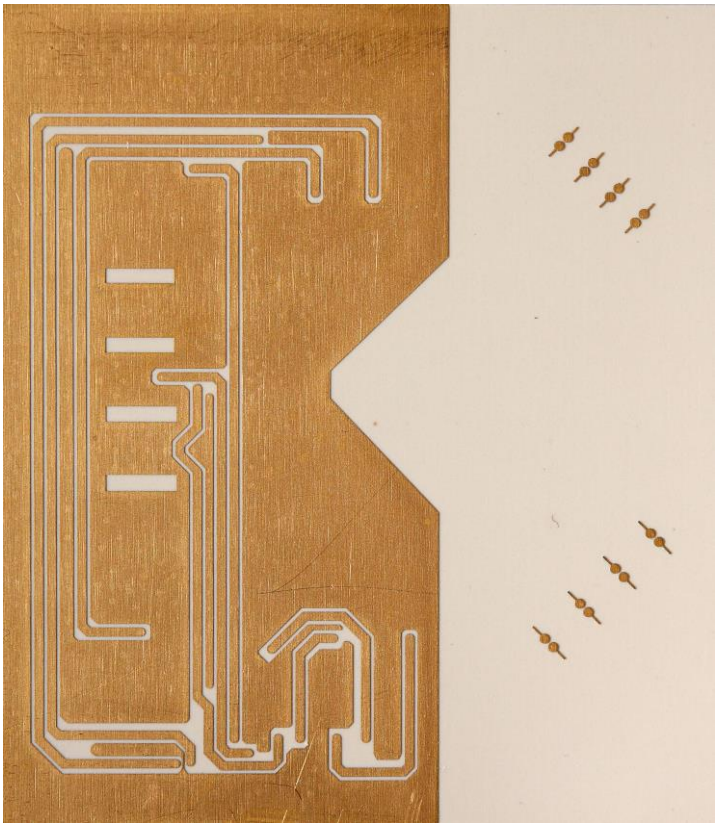

(c)

Figure 54. Fabricated package: (a) Top-view of ML1; (b) ML1 zoomed-view of chip pads and coplanar transition to microstrip; (c) Bottom-view (ML3).

A multilayer organic (MLO) package complete with routing, transitions and bonding was done for the RF CMOS chip. The transitions and bonding involved were carefully chosen based on the chip's requirement and the high performance techniques found in Chapter 3. The orientation of the arrays incorporated in the package was selected based on the results in Chapter 4.1. With all the previously mentioned details and fabricated structures depicted in Figure 54, the MLO package is now complete.

CHAPTER 5:

CONCLUSIONS

RF characterization was done for the first time on several promising organic and 3D-printed substrates. The newly characterized data were validated through various RF designs. Based on the validated results, a multilayer organic stack-up was chosen to carry out a full integration with an RF CMOS chip. For the package, three different mm-wave antenna configurations were analyzed and measured. Results for the 0° configurations reveal the E-plane cuts were clean, but the corresponding H-planes suffered significant ripples. The 90° configurations had the opposite effect. The 45° configuration presents the best compromise, having good results for both pattern cuts. Increasing the distance between the configurations reduced either the amount of ripples or their average level. However, it also reduced the gain by ~0.5 dB and increased the overall size by 5 mm in both x and y directions. This tradeoff between smoother patterns with less gain fluctuations at a lower gain level and a larger package should be taken into account when integrating antenna designs together. Incorporating the guidelines summarized in Chapter 4 (p. 73) into dual packaged antennas will significantly reduce inter-array influence, and, for those simultaneously excited, will guarantee better performance in high speed mm-wave wireless communication systems.

The designed package was able to combine all the required components without compromising RF performance for the arrays. This is in stark contrast to on-chip solutions, which need more involved methods or costly post-processing techniques to alleviate losses

related to surface waves. In this regard, a system-on-package solution shows more promise for millimeter-wave communications. Organic substrates like LCP continue to showcase the ability to create high-performance packages, especially as we move up in frequency.

New developments using the organic substrates at lower frequencies (915 MHz) were also achieved. For the first time, a microfluidic channel embedded in organics was created and used as a size reducing technique. The filled channel substantially reduced the size of the antenna designs, yielding a length reduction of over 44% and an area reduction of 54%. This simple and versatile approach can be easily employed in conjunction with other size reduction techniques for a low-cost, planar, and compact RF front-end solution.

Finally, thin film characterization of popular 3D-printed ABS substrates was provided for the first time above 11 GHz using a cavity resonator. It was further demonstrated, also for the first time, that an antenna above 20 GHz on ABS can be fabricated through direct print additive manufacturing micro-dispensing method. These results open a world of possibilities for additive manufacturing technologies in the RF world at high frequencies.

CHAPTER 6:

FUTURE WORK

6.1 Further Studies for packaged RF CMOS chip

Through the researched orientation study and multi-layer integration, the complete packaged system was achieved. Future work for the packaged solution should focus on two main goals: researching any differences in end-fire array designs, and performing an exhaustive study for different scenarios while performing transmission measurements. These should include:

- Transmission distance variations between Tx and Rx modules
- Different angles (or orientations)
- Various modulation schemes
- Transmission of different file modes

Carrying out all of the above will provide a complete validation of the RF CMOS chip. Ultimately, all of these will demonstrate the package is not only novel and functional, but also ready to be used in today's communication systems.

LOWER FREQUENCY STUDIES AND PACKAGE FEASIBILITY

To keep a compact package profile and allow for broadband performance, gold bumps were be used in the multi-layer CMOS chip integration in Chapter 4, Section 2. This was necessary given the desired bandwidth and operating frequencies. However, at lower

frequencies where the losses are more reasonable, it would be possible to have to have a wirebond solution as well. Of course, depending on the actual frequencies of the chip, wirebonds might still present bandwidth limitations for dual excitation. Analyzing and comparing the performance of both packaged solutions will provide greater insight of the package and serve to expand its bandwidth versatility. Different RF chips could also be incorporated into a similar package for comparison.

6.2 3D-printing in the RF world

Having the dielectric properties of ABS at a higher frequency enables us to design many RF devices in this frequency range. More work should focus on using additive printing techniques to fabricate other RF designs. Characterization should also go beyond ABS and extend to various commonly used 3D-printing materials. For higher frequencies, the characterization should focus on thin film materials (under 1.0 mm). Given its low cost and ease of fabrication, the frequency and minimum feature size limits of this particular 3D-printing technique should be thoroughly investigated.

REFERENCES

[1] White House Press Release: "President Obama Details Plan to Win the Future through Expanded Wireless Access". Available: http://www.whitehouse.gov/the-press-office/2011/02/10/president-obama-details-plan-win-future-through-expanded-wireless-access. February 2011.

[2] D. C. Thompson, et al, "Characterization of Liquid Crystal Polymer (LCP) Material and Transmission Lines on LCP Substrates from 30 to 110 GHz," *IEEE Transactions Microwave Theory and Techniques*, vol. 52, issue 4, pp. 1342-1352, April 2004.

[3] A. Amadjikpe, A. Vera, D. Choudhury and J. Papapolymerou, "Study of a 60 GHz Rectangular Patch Antenna on a Flexible LCP Substrate for Mobile Applications," *2008 IEEE Antennas and Propagation Society International Symposium*, pp. 1-4, July 2008.

[4] G. Zou, et al, "High Frequency Characteristics of Liquid Crystal Polymer for System in a Package Application," *IEEE 8th International Advanced Packaging Materials Symposium*, pp. 337-341, March 2002.

[5] Y. P. Zhang and Duixian Liu, "Antenna-on-Chip and Antenna-in-Package Solutions to Highly Integrated Millimeter-Wave Devices for Wireless Communications," *IEEE Transactions on Antennas and Propagation*, vol. 57, no. 10, pp. 2830-2841, October 2009.

[6] Y. P. Zhang, et. al, "Antenna-in-Package Design for Wirebond Interconnection to Highly Integrated 60-GHz radios," *IEEE Transactions on Antennas and Propagation*, vol. 57, no. 10, pp. 2842-2852, Oct. 2009.

[7] G. Felic and S. Skafidas, "Flip-Chip Interconnection Effects on 60-GHz Microstrip Antenna Performance," *Antennas and Wireless Propagation Letters*, IEEE, vol. 8, pp. 283-286, 2009.

[8] F. Gutierrez et al., "On-chip Integrated Antenna Structures in CMOS for 60 GHz WPAN Systems," *IEEE Journal on SAC*, vol. 27, issue 8, pp. 1367-1378, 2009.

[9] A. Amadjikpe, D. Choudhury, G. E. Ponchak, and J. Papapolymerou, "60-GHz Switched-beam End-fire Antenna Module Integrated with Novel Microstrip-to-Slot Transition," *Microwave Symposium Digest (MTT), 2011 IEEE MTT-S International*, pp. 1-4, June 2011.

[10] C. E. Patterson, T. K. Thrivikraman, S. K. Bhattacharya, C. T. Coen, J. D. Cressler and J. Papapolymerou, "Development of a multilayer organic packaging technique for a fully embedded T/R module," in *Proc. EuMC* 2011, pp. 261-264, October 2011.

[11] A. Valdes-García, S. Nicolson, J. W. Lai, A. Natarajan, P.-Y. Chen, S. Reynolds, J. H. C. Zhan, D. Kam, D. Liu and B. Floyd, "A Fully Integrated 16-element Phased Array Transmitter in SiGe BiCMOS for 60-GHz Communications," *IEEE Journal of Solid-State Circuits*, vol. 45, no. 12, pp. 2757-2773, December 2010.

[12] W. Khan, S. Bhattacharya, C. Patterson, G. Ponchak and J. Papapolymerou, "Low Cost 60 GHz RF-Front End Transceiver Integrated on Organic Substrate," *2011 IEEE MTT-S International*, pp. 1-4, June 2011.

[13] L. Chen, T. Zhang, S. Liu, and X. Shi, "A Bidirectional Dual-Frequency Retrodirective Array for Full-Duplex Communication Applications," *IEEE Antennas and Wireless Propagation Letters*, vol. 11, pp. 771-774, June 2012.

[14] G. S. Shiroma, R.Y. Miyamoto, and W.A. Shiroma, "A Full-Duplex Dual-Frequency Self-Steering Array Using Phase Detection and Phase Shifting," *IEEE Transactions on Microwave Theory and Techniques*, vol. 54, pp. 128-134, January 2006.

[15] K. Kawasaki et al., "A Millimeter-Wave Intra-Connect Solution," *IEEE Journal of Solid-State Circuits*, vol. 45, no. 12, pp. 2655-2666, December 2010.

[16] S. Fukada et al., "A 12.5+12.5Gb/s Full-Duplex Plastic Waveguide Interconnect," *IEEE Journal of Solid-State Circuits*, vol. 46, no. 12, pp. 3113-3125, December 2011.

[17] Y. Tanaka et al., "A Versatile Multi-Modality Serial Link," *2012 IEEE International Solid-State Circuits Conference*, pp. 332-334, Feb. 2012.

[18] A. Valdes-García, et al., "Single-Element and Phased-Array Transceiver Chips for 60-GHz Gb/s Communications", *Integrated Circuits and Communications IEEE Communications Magazine*, pp. 120-131, April 2011.

[19] A. Valdes-García, et al., "Multi-Mode Modulator and Frequency Demodulator Circuits for Gb/s Data Rate 60 GHz Wireless Transceivers," *IEEE Custom Integrated Circuits Conference*, pp. 639-642, 2007.

[20] B. Floyd, et al., "Silicon Millimeter-Wave Radio Circuits at 60-100 GHz," invited to the *2007 Topical Meeting on Silicon Monolithic Integrated Circuits in RF Systems*, pp.213-218, January 2007.

[21] M. Sun, Y. P. Zhang, "A 60-GHz LTCC Microstrip Grid Array Antenna," *Asia Pacific Microwave Conference*, Yokohama, Japan, pp. 1673-1676, 2010.

[22] E. Cohen, C.G. Jakobson, S. Ravid, and D. Ritter, "A Bidirectional Tx/Rx Four-element Phased Array at 60 GHz with RF-IF Conversion Block in 90nm CMOS Process," *IEEE Trans. Microw. Theory Tech.*, vol. 58, no.5, pp. 1438–1446, May 2010.

[23] E. Cohen, M. Ruberto, M. Cohen, O. Degani, S. Ravid, and D. Ritter, "A CMOS Bidirectional 32-element Phased-array Transceiver at 60 GHz with LTCC Antenna," *IEEE Radio Freq. Integr. Circuits Symp.*, pp. 439-442, June 2012.

[24] W. T. Khan, C. Ulusoy and J. Papapolymerou, "D- Band Characterization of Co-Planar Wave Guide and Microstrip Transmission Lines on Liquid Crystal Polymer," *IEEE Electronic Components and Technology Conference*, pp. 2304-2309, May 2013.

[25] C. Patterson, W.T. Khan, G.E. Ponchak, G.S. May and J. Papapolymerou, "A 60-GHz Active Receiving Switched-Beam Antenna Array with Integrated Butler Matrix and GaAs Amplifiers," *IEEE Transactions on Microwave Theory and Techniques*, vol. 60, no. 11, pp. 3599-3607, November 2012.

[26] D. Chung, A. L. Amadjikpe and J. Papapolymerou, "Multilayer Integration of Low-Cost 60-GHz Front-End Transceiver on Organic LCP," *IEEE Antennas and Wireless Propagation Letters*, vol. 10, pp. 1329-1332, November 2011.

[27] A. L. Vera López, W. T. Khan and J. Papapolymerou, "Orientation Study to Minimize Coupling Effects of Dual-Packaged Millimeter-Wave Antennas," *IET Microwaves, Antennas & Propagation*, vol. 9, issue 2, pp.159-165, January 2015.

[28] A. Vera López, S. Bhattacharya, C. Donado Morcillo, J. Papapolymerou, D. Choudhury, and A. Horn, "Novel Low Loss Thin Film Materials for Wireless 60 GHz Applications," *Proceedings for IEEE 60th Electronic Components and Technology Conference*, Las Vegas, NV, USA, pp. 1990-1995, June 2010.

[29] S. A. Ivanov, V. N. Peshlov, "Ring-Resonator Method Effective Procedure for Investigation of Microstrip Line," *IEEE Microwave and Wireless Components Letters*, vol. 13, no. 6, pp. 244-246, June 2003.

[30] S. Hwang, S. Min, "Characterization of Next Generation Thin Low-k and Low-loss Dielectrics from 1 to 110 GHz", *IEEE Transactions on Advanced Packaging*, vol. 33, no. 1, pp. 180-188, February 2010.

[31] J. M. Heinola, and K. Tolsa, "Dielectric Characterization of Printed Wiring Board Materials Using Ring Resonator Techniques: A Comparison of Calculation Models," *IEEE Transactions on Dielectrics and Electrical Insulation*, vol. 13, no. 4, pp. 717-726, August 2006.

[32] G. Zheng, J. Papapolymerou, and M. M. Tentzeris, "Wideband Coplanar Waveguide RF Probe Pad to Microstrip Transitions Without Via Holes," *IEEE Microwave and Wireless Components Letters*, vol. 13, no. 12, pp. 544-546, December 2003.

[33] L. Martens, "High-frequency Characterization of Electronic Packaging," Kluwer Academic Publishers, pp. 51-53, 109-111, 1998.

[34] C. Donado Morcillo, S. Bhattacharya, A. Horn, and J. Papapolymerou, "Conductor Surface-Roughness Effect in the Loss Tangent Measurement of Low-Loss Organic Substrates from 30 GHz to 70 GHz," *Proc. 60th Electronic Components and Technology Conference*, pp. 727-734, June 2010.

[35] E. Macdonald, R. Salas, D. Espalin, M. Perez, E. Aguilera, D. Muse, and R.B. Wicker, "3D Printing for Rapid Prototyping of Structural Electronics," *IEEE Access*, vol. 2, pp. 234-242, March 2014.

[36] L. Novakova-Marcincinova, J. Novak-Marcincin, J. Barna, and J. Torok, "Special Materials Used in FDM Rapid Prototyping Technology Application," 2012 IEEE International Conference on Intelligent Engineering Systems (INES), pp. 73-76, June 2012.

[37] B. Riddle, J. Baker-Jarvis, J. Krupka, "Complex Permittivity Measurements of Common Plastics Over Variable Temperatures," *IEEE Transactions on Microwave Theory and Techniques*, vol. 51, no. 3, 727-733, March 2003.

[38] P.I. Deffenbaugh, R.C. Rumpf, K.H. Church, "Broadband Microwave Frequency Characterization of 3-D Printed Materials," *IEEE Transactions on Components, Packaging and Manufacturing Technology*, vol. 3, no. 12, pp. 2147-2155, December 2013.

[39] A. Bisognin, D. Titz, F. Ferrero, R. Pilard, C.A. Fernandes, J.R. Costa, C. Corre, P. Calascibetta, J.M. Riviere, A. Poulain, C. Badard, F. Gianesello, C. Luxey, P. Busson, D. Gloria, and D. Belot, "3D Printed Plastic 60 GHz Lens: Enabling Innovative Millimeter Wave Antenna Solution System," 2014 IEEE International Microwave Symposium (IMS), pp. 1-4, June 2014.

[40] I.T. Nassar, T.M. Weller, and H. Tsang, "A 3D-Printed Miniaturized Log-Periodic Dipole Antenna," 2014 IEEE Antennas and Propagation Society International Symposium (APSURSI), pp. 11-12, July 2014.

[41] E.A. Rojas-Nastrucci, T. Weller, A. Vera-López, F. Cai, and J. Papapolymerou, "A Study on 3D-Printer Coplanar Waveguide with Meshed and Finite Ground Planes," *2014 IEEE Wireless and Microwave Technology Conference (WAMICON)*, pp. 1-3, June 2014.

[42] A. Vera López**,** E.A. Rojas-Nastrucci, M. Córdoba-Erazo, T. Weller, and J. Papapolymerou, "Ka-Band Characterization and RF Design of Acrylonitrile Butadiene Styrene (ABS)," *2015 IEEE International Microwave Symposium*, pp. 1-4, May 2015.

[43] D. M. Pozar, "A Review of Aperture Coupled Microstrip Antennas: History, Operation, Development and Application," University of Massachusetts at Amherst, MA, May 1996.

[44] A. L. Vera López, D.B. Giles, W.T. Khan, O. Chlieh, G.E. Ponchak and J. Papapolymerou, "Microfluidic Channel on Organic Substrate as Size Reducing

Technique for 915 MHz Antenna Designs," Proceedings IEEE 2013 Asia Pacific Microwave Conference (APMC), pp. 1181-1184, 2013.

[45] F. Farzami, K. Forooraghi, M. Norooziarab, "Miniaturization of a microstrip antenna using a compact and thin magneto-dielectric substrate," *Antennas and Wireless Prop. Letters, IEEE,* vol. 10, pp. 1540-1542, 2011.

[46] M. Abedian, S. K. A. Rahim, M. Khalily, "Two-segments compact dielectric resonator antenna for UWB application," *Antennas and Wireless Prop. Letters, IEEE,* vol. 11, pp. 1533-1536, 2012.

[47] D. Psychoudakis, J. L. Volakis, "Conformal asymmetric meandered flare (AMF) antenna for body-worn applications," *Antennas and Wireless Prop. Letters, IEEE,* vol. 8, pp. 931-934, 2009.

[48] J. P. Gianvittorio, Y. Rahmat-Samii, "Fractal antennas: a novel antenna miniaturization technique, and applications," *Antennas and Prop. Magazine, IEEE,* vol. 44, no. 1, pp. 20-36, 2002.

[49] R. Buchner, J. Barthel, and J. Stauber, "The dielectric relaxation of water between 0 C and 35 C," *Chem. Phys. Lett.*, vol. 306, no. 1–2, pp. 57-63, Jun. 1999.

[50] O.L. Chlieh, W.T. Khan, J. Papapolymerou, "L-Band Tunable Microstrip Bandpass Filter on Multilayer Organic Substrate with Integrated Microfluidic Channel," 2014 *IEEE MTT-S Int. Microwave Symp. Dig.,* pp. 1-4, June 2014.

[51] A. L. Vera Lopez, A. Akiba, K. Ikeda, S. Mitarai, G. E. Ponchak, J. Papapolymerou, "Hybrid silicon-organic packaged antenna array at 60 and 80 GHz using a low-cost bonding technique," 2012 *IEEE MTT-S Int. Microwave Symp. Dig.,* pp. 1-3, June 2012.

[52] D. Thompson, M. M. Tentzeris, J. Papapolymerou, "Experimental analysis of the water absorption effects on RF/mm-wave active/passive circuits packaged in multilayer organic substrates," *IEEE Trans. on Advanced Packaging,* vol. 30, no. 3, pp. 551-557, Aug. 2007.

[53] I. Papapolymerou, R. Drayton, and L. Katehi, "Micromachined Patch Antennas,'' *IEEE Transactions on Antennas and Propagation*, vol. 46, no. 2, pp. 275-283, February 1998.

[54] P. Sharma, S. K. Koul and S. Chandra, "Micromachined Inset-Fed Patch Antenna at Ka-Band," *Proceedings of Asian-Pacific Microwave Conference*, pp. 693-696, 2006.

[55] V. K. Singh, "Ka-Band Micromachined Microstrip Patch Antenna," *EIT Microwaves Antenna and Propagation*, vol. 4, issue 3, pp. 316-323, 2010.

[56] A. Vera López, A. Akiba, K. Ikeda, S. Mitarai, G. E. Ponchak and J. Papapolymerou, "60 GHz Micromachined Patch Antenna for Wireless Applications," *2011 IEEE International Symposium on Antennas and Propagation*, pp. 515-518, July 2011.

[57] A. V. Sathanur, K. J. Vinoy, "A Design Procedure for Micromachined Antennas on Semiconductor Substrates", *IEEE Indicon Conference*, pp. 203-207, December 2005.

[58] C. E. Patterson, S. K. Bhattacharya, J. Zepess, S. Leiphart, W. G. Trueheart, J. Ajoian, Z. Coffman and J. Papapolymerou, "A 7.45 GHz BAW filter on a Low Cost 3D Organic Package," *2011 IEEE MTT-S Int. Microwave Symp. Dig.*, pp. 1-4, June 2011.

[59] A. Amadjikpe, D. Choudhury, G. E. Ponchak and J. Papapolymerou, "Highly Directive Package-Integrated Dipole Arrays for 60-GHz Front End Modules," *2010 IEEE MTT-S Int. Microwave Symp. Dig.*, pp. 348-351, May 2010.

[60] A. Vera López, W. T. Khan and J. Papapolymerou, "Dual Frequency Organically Packaged Antenna Arrays at 57 and 80 GHz," *2013 IEEE Int. Microwave Symposium*, pp. 1-4, June 2013.

Aida Luz Vera-López

11 Rius Rivera Street
Adjuntas, Puerto Rico 00601
Mobile: (787) 484 – 1173

18582 NW Holly Street
Hillsboro, OR 97006
avera3@gatech.edu

EDUCATION

Georgia Institute of Technology
Ph D in Electrical Engineering and Computer Engineering
Minor in Material Science
Dissertation: "Dual-band Lightweight, Low-cost RF Front-end Solutions for Point-to-point Wireless Applications"

Georgia Institute of Technology
Master of Science in Electrical and Computer Engineering
Minor in Material Science
GPA – 3.90/4.00

University of Puerto Rico, Mayagüez
Baccalaureate in Sciences in Electrical Engineering
Specialization: Applied Electromagnetics
Summa Cum Laude
GPA – 4.00/4.00

SKILLS

- Software tools: Ansoft High Frequency Structural Simulator (HFSS), Agilent Advanced Design System (ADS), COMSOL, PSpice, LogicWorks, NEC-Win, AutoCad, Matlab, Mathematica
- Measurement tools: Network and spectrum analyzer, anechoic chamber antenna measurements
- Possess basic cleanroom training (machines: spin coater, wet-etching, mask aligner)
- Passed FE Electrical and Computer Exam - National Council of Examiners for Engineering and Surveying (NCEES)
- Languages: Spanish (native), English, Italian (intermediate)

EXPERIENCE

Industry

Rotation Engineer, Intel Corporation - Wireless Charging Group

- PCB coil design, optimization and measurement

Systems Engineer Intern, Johns Hopkins University Applied Physics Laboratory

- Radar cross section modeling

Systems Engineer, Johns Hopkins University Applied Physics Laboratory

- Radar cross section modeling

Research

Research Assistant, Georgia Institute of Technology - Microwave Circuit Technology Group, Advisor: Dr. John Papapolymerou

- Design, simulation, integration and measurement of RF devices

Research Assistant, University of Puerto Rico Mayagüez - Collaborative Adaptive Sensing of the Atmosphere (CASA)

- Wireless link design for radar data acquisition
- Radio propagation analysis for the study of terrain profiles

Volunteer Research, University of Puerto Rico Mayagüez - Lightning Detection Study

- Analysis and processing of lightning activity data

Teaching

Teaching Assistant, Georgia Institute of Technology

- Electromagnetics; involved grading, holding office hours, proctoring exams, planning lectures and teaching sporadically

Teaching Assistant, University of Puerto Rico Mayagüez

- Control Systems class; involved grading, holding office hours, proctoring exams

Volunteer Math Tutor, University of Puerto Rico Ponce

- Prepared practice exercises, tutored and assisted students in various Math courses

HONORS AND AWARDS

- Tech Tower Award (Spring 2009 and Spring 2014)
- Honorable mention in Best Student Paper Competition at the 2012 IEEE International Microwave Symposium (IMS)
- Invitation to Gamma Beta Phi Honor Society
- Invitation to Eta Kappa Nu Electrical and Computer Engineering Honor Society
- Xerox Technical Minority Scholarship recipient
- Goizueta Fellow
- GEM Fellow

- Engineering Faculty Award to Student with Highest Academic Index (UPR Mayagüez)
- Ranked 1 out of 184 students in the Electrical and Computer Engineering Department at the University of Puerto Rico Mayagüez graduation
- Summa Cum Laude (UPR Mayagüez)
- Tau Beta Pi Engineering Honor Society Membership nomination
- Dean's List and Honor Tuition

PUBLICATIONS

- **A. Vera López,** E.A. Rojas-Nastrucci, M. Córdoba-Erazo, T. Weller, and J. Papapolymerou, "Ka-Band Characterization and RF Design of Acrylonitrile Butadiene Styrene (ABS)," *2015 IEEE International Microwave Symposium*, pp. 1-4, May 2015.
- **A. Vera López,** W. T. Khan and J. Papapolymerou, "Orientation Study to Minimize Coupling Effects of Dual-Packaged Millimeter-Wave Antennas," *IET Microwaves, Antennas & Propagation Journal*, vol. 9, Issue 2, pp. 159-165, January 2015.
- S. Zeinolabedinzadeh, **A. Vera López**, N.E. Lourenco, A.C. Ulusoy, M. Kaynak, M. Kamarei, B. Tillack, J. Papapolymerou, and J.D. Cressler "A 2×2, 316 GHz SiGe Scalable Transmitter Array with Novel Phase Locking Method and On-die Antennas," *2014 IEEE Bipolar/BiCMOS Circuits and Technology Meeting (BCTM)*, pp. 60-63, September 2014.
- E.A. Rojas-Nastrucci, T. Weller, **A. Vera López**, F. Cai and J. Papapolymerou, "A Study on 3D-Printed Coplanar Waveguide with Meshed and Finite Ground Planes," *Proceedings 2014 IEEE 15th Annual Wireless and Microwave Technology Conference (WAMICON)*, pp. 1-3, June 2014.
- W.T. Khan, **A. Vera López**, C. Ulusoy, and J. Papapolymerou, "Packaging a W-Band Integrated Module with an Optimized Flip-Chip Interconnect on an Organic Substrate," *IEEE Transactions on Microwave Theory and Techniques (MTT)*, vol. 62, issue 1, pp. 64-72, January 2014.
- **A. Vera López,** D.B. Giles, W.T. Khan, O. Chlieh, and J. Papapolymerou, "Microfluidic Channel on Organic Substrates as Size Reducing Technique for 915 MHz Antenna Designs," 2013 *IEEE Asia Pacific Microwave Conference*, pp. 1181-1184, November 2013.
- S.C. Kwon, G.L. Stüber, **A. Vera López,** and J. Papapolymerou, "Geometrically Based Statistical Model for Polarized Body Area-Network Channels," *IEEE Transactions on Vehicular Technology*, vol. 62, issue 8, pp. 3518-3530, October 2013.
- S.C. Kwon, G.L. Stüber, **A. Vera López,** and J. Papapolymerou, "Geometrically Based Statistical Model for Polarized Body Area Network Channels," *Proceedings*

of the Tenth International Symposium on Wireless Communication Systems (ISWCS), pp. 1-5, August 2013.

- W.T. Khan, **A.L. Vera López**, G.E. Ponchak and J. Papapolymerou, "Integration of V-Band and W-Band Antennas with SPDT Switch on Organic Substrate," *Proceedings of 2013 IEEE Antennas and Propagation Society International Symposium (APSURSI)*, pp. 666-667, July 2013.
- **A. Vera López,** W.T. Khan, A. Akiba, K. Ikeda, H. Mitsuo, and J. Papapolymerou, "Dual Frequency Organically Packaged Antenna Array at 57 and 80 GHz," *2013 IEEE International Microwave Symposium*, pp. 1-4, June 2013.
- ***A. Vera López,** A. Akiba, K. Ikeda, S. Mitarai, G.E. Ponchak, and J. Papapolymerou, "Hybrid Silicon-Organic Packaged Antenna Array at 60 and 80 GHz Using a Low-Cost Bonding Technique," *2012 IEEE International Microwave Symposium*, pp. 1-4, 2012.
  **** Honorable Mention Best Student Paper Competition (Top 10)***
- **A. Vera López,** J. Papapolymerou, A. Akiba, K. Ikeda, S. Mitarai, G.E. Ponchak, "60 GHz Micromachined Patch Antenna for Wireless Applications," *2011 IEEE AP-S International Symposium on Antennas and Propagation*, pp. 515-518, 2011.
- **A. Vera López,** S. Bhattacharya, C. Donado Morcillo, J. Papapolymerou, D. Choudhury, and A. Horn, "Novel Low Loss Thin Film Materials for Wireless 60 GHz Applications," *IEEE 60th Electronic Components and Technology Conference*, pp. 1990-1995, 2010.
- Arnaud Amadjikpe, **A. Vera**, D. Choudhury and J. Papapolymerou, "Study of a 60 GHz Rectangular Patch Antenna on a Flexible LCP Substrate for Mobile Applications," *Proceedings of IEEE's 2008 Antennas and Propagation Society International Symposium (AP-S)*, pp. 1-4, July 2008.

ACTIVITIES AND MEMBERSHIPS

- Member of the Institute of Electrical and Electronics Engineers (IEEE)
- Member of the Society of Hispanic Professional Engineers **(**SHPE**)**
- Member of the Society of Women Engineers **(**SWE**)**
- President of the Student's Math Association (UPR Ponce)